Research Highlights

- An "integrated" holistic approach for structural health monitoring of masonry arch bridges
- Non-destructive assessment using multi-source, multi-scale and multi-temporal information
- Use of high-frequency (2000 MHz) and low-frequency (200-600 MHz) GPR antenna systems
- Use of the Interferometric Synthetic Aperture Radar (InSAR – C-band sensors) technique
- A case study (the "Old Bridge" at Aylesford, Kent, UK– a 13th century bridge) is presented

An Integrated Investigative Approach in Health Monitoring of Masonry Arch Bridges Using GPR and InSAR Technologies

Amir M. ALANI[1], Fabio TOSTI[1]*, Luca BIANCHINI CIAMPOLI[2], Valerio GAGLIARDI[2] and Andrea BENEDETTO[2]

[1]*School of Computing and Engineering, University of West London (UWL), St Mary's Road, Ealing, London W5 5RF, UK e-mail: Amir.Alani@uwl.ac.uk; Fabio.Tosti@uwl.ac.uk (*Corresponding author)*

[2]*Department of Engineering, Roma Tre University, Via Vito Volterra 62, 00146, Rome, Italy e-mail: luca.bianchiniciampoli@uniroma3.it; valerio.gagliardi@uniroma3.it; andrea.benedetto@uniroma3.it*

Abstract

This paper provides an overview of the existing health monitoring and assessment methods for masonry arch bridges. In addition, a novel "integrated" holistic non-destructive approach for structural monitoring of bridges using ground-based non-destructive testing (NDT) and the satellite remote sensing techniques is presented. The first part of the paper reports a review of masonry arch bridges and the main issues in terms of structural behaviour and functionality as well as the main assessment methods to identify structural integrity-related issues. A new surveying methodology is proposed based on the integration of multi-source, multi-scale and multi-temporal information collected using the Ground Penetrating Radar (GPR – 200, 600 and 2000 MHz central frequency antennas) and the Interferometric Synthetic Aperture Radar (InSAR – C-band SAR sensors) techniques. A case study (the "Old Bridge" at Aylesford, Kent, UK – a 13th century bridge) is presented demonstrating the effectiveness of the proposed method in the assessment of masonry arch bridges. GPR has proven essential at providing structural detailing in terms of subsurface geometry of the superstructure as well as the exact positioning of the structural ties. InSAR has identified measures of structural displacements caused by the seasonal variation of the water level in the river and the river bed soil expansions. The above process forms the basis for the "integrated" holistic structural health monitoring approach proposed by this paper.

Keywords: masonry arch bridges, "integrated" holistic structural health monitoring approach; non-destructive testing (NDT) assessment, ground penetrating radar (GPR); Interferometric Synthetic Aperture Radar (InSAR); Remote Sensing monitoring

1   Introduction

Arch bridge structures are very common and historical types of asset vital to the economy, mobility and development of communities. The oldest example of an arch bridge is the Mycenaean bridge of Kazarma, dating back to 1300 BC and still partially operational. From that time onwards, stones and

48 bricks have been used as primary construction materials for arch bridges up to the steel revolution
49 period, when iron became the more dominant structural material.

50 Masonry arch bridges are very solid and compact forms of structures, suitable to resist floods and
51 time degradation. In this regard, a comprehensive research by [1] counted 931 Roman masonry arch
52 bridges in 26 different European countries, with many of them still standing and used to carry
53 vehicles.

54 No doubt an effective assessment and routine monitoring of bridge structures are nowadays crucial
55 for maintenance, regardless of their historical value and mobility function. As an example, more
56 recent reinforced concrete structures require routine, precise and reliable monitoring due to
57 increasing traffic volumes and operational speeds of transports. On the other hand, historical
58 bridges, and mostly arch bridges, represent a cultural heritage asset where sampling or digging parts
59 of the structures is often constrained for structural investigations.

60 Non-destructive testing (NDT) methods are being increasingly used to meet the above requirements
61 for assessment and monitoring of modern and historical bridges during their service-life period. In
62 this regard, efforts have been dedicated to the monitoring of dynamic responses of bridges,
63 including deflections and displacements induced by thermal expansions and vibrations. Health of
64 bridges can be assessed using various monitoring methods and sensors, such as ground penetrating
65 radar (GPR), GPS, accelerometers and levelling [2-5]. Recent applications of the ground-based
66 microwave interferometry have been also reported in the literature for both static and dynamic
67 monitoring of bridges [6-7]. However, constraints given by installation costs of in-contact sensors
68 and time duration of periodical field surveys have not allowed collection of time-series monitoring
69 for many bridges in the long term.

70 Scour and differential settlements of bridge decks are also elements of major concerns for their
71 structural integrity [8-9]. Scour is defined as the excavation and removal of material from the bed
72 and banks of streams as a result of the erosive action of flowing water [10] . This action in the vicinity
73 of bridge piers can cause removal of ground material at the foundation level, increasing the risk of
74 structural collapse. This occurrence can be emphasised by changes in water flow rates during
75 flooding that can affect the structural stability of bridge piers. According to Prendergast and Gavin
76 [11], scour can be monitored by a range of instrumentation including single-use devices, pulse or
77 radar devices, buried or driven rod systems, sound-wave devices, fiber-Bragg grating devices and
78 electrical conductivity equipment. However, information available from the literature on this type
79 of failure have proven that collapse for many of these structures (more than 600) can verify in a
80 relatively short period of a few decades [12,13]. These figures also confirm that stand-alone and
81 integrated use of ground-based techniques, including NDT methods, does not represent the most
82 comprehensive solution to this specific structural issue.

83 Within this context, use of satellite data-based synthetic aperture radar (SAR) interferometry
84 (InSAR) has proven to be effective at measuring displacements of infrastructures and natural terrain.
85 A main advantage of this technique is that millimetre-scale changes of multiple discrete points can
86 be monitored remotely in time and over large spatial areas [14-15]. Early-stage use of InSAR was in
87 the analyses of large-scale deformations caused by earthquakes or vulcanoes with several spatial
88 resolution constraints [16]. This drawback was addressed by the use of recently-developed C-band
89 SAR sensors, with a centimetre accuracy and a higher availability of images with a wider spatial

coverage, as well as the X-band SAR sensors, working in the X-band range. X-band SAR sensors are capable to collect images with a higher spatial resolution providing measurements with a millimetre accuracy. In addition, the considerable amount of orbiting SAR sensors have allowed acquisition of satellite images with a very short temporal baseline [17]. These improvements have recently contributed to a tremendous increase of applications to linear infrastructures [18,19] and bridges [20-24]. On the other hand, it worth emphasising that stand-alone use of the InSAR technique cannot be accounted as a unique solution for providing comprehensive structural health monitoring, as no information can be collected on the source of damage [18].

Within this framework, it is the opinion of the Authors that a more comprehensive structural health monitoring strategy can be pursued by the integration of multi-source, multi-scale and multi-temporal information collected using ground-based non-destructive testing (NDT) methods and satellite remote sensing. This is more emphasised in the case of historical bridges, where use of traditional destructive techniques is often constrained for conservation purposes and time of intervention is crucial to avoid irreversible and inestimable structural failure.

2   Aim and Objectives

The main aim of this paper is to investigate the potential of integrating information from satellite remote sensing and ground-based non-destructive methods for a comprehensive monitoring of historical masonry arch bridges subject to seasonal changing patterns (variations of the water flow level of rivers crossed). To achieve this aim, the following objectives are identified:

- to provide a good overview on main structural issues in masonry arch bridges in order to identify advantages and limitations of existing assessment methods (i.e., conventional and non-destructive);

- to prove the viability of using GPR as a rapid and effective NDT technique in providing structural detailing of the bridge deck. To this purpose, applicability of high-frequency and low-frequency antenna systems was investigated to achieve structural information such as thickness and geometry of bridge components and the exact positioning of the structural ties at different depths and resolutions;

- to assess amount of displacements of the bridge structure linked with seasonal variations of the water flow level of the river crossed by the bridge;

- to test the feasibility of the Permanent Scatterers Intereferometry (PSI) technique in bridge monitoring applied to a medium-range ground-resolution datasets (i.e., C-band), paving the way to future implementations using higher resolution sensors (e.g., X-band).

3   Masonry Bridges

Masonry is defined as a structural material made by the assemblage of natural (stones) or artificial (bricks) elements, with or without mortar, suitable for the realisation of the bearing elements of a structure [25]. In view of a similar morphology, brick bridges should be analysed together with stone bridges as a part of them [26]. The typical structure of a masonry arch bridge is shown in Figure 1.
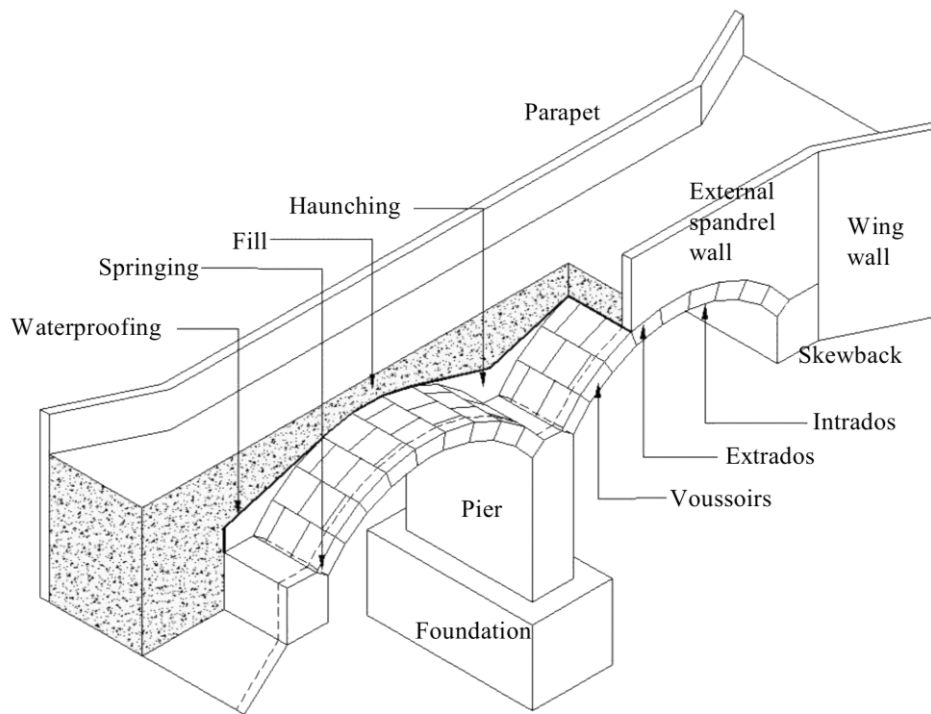
130   **Fig. 1** Main elements of a masonry arch bridge (UIC Code 778-3R) [27].

131   Stone arch bridges rely on several advantages compared to concrete bridges. A larger proportion of
132   locally available resources are used in stone bridges as they can be built with local labour and stones.
133   On the contrary, raw materials and machines have to be moved on site for the construction of
134   concrete bridges and specialised technical expertise are required. Compared to expensive
135   aggregates, local stones are strong and affordable materials often available in the vicinity of the
136   construction site. In regard to the construction costs, concrete bridges require more investments and
137   use of specialist equipment that do not compensate for the cost of additional man-days usually
138   required for the construction of stone arch bridges. Risk of floods washing the stone arch culverts
139   away is reduced by their own weight. In addition, the interconnecting arch and the heavy weight
140   prevent typical technical challenges related to concrete bridge abutments (i.e., the tilting and sliding
141   exerted by the backfilled soil mass).

142   Nevertheless, concrete bridges appear as a more suitable technology option in case of higher labour
143   costs and larger spans are involved. In this regard, the maximum single span in stone bridges is
144   usually less than 20 meters. In case of larger single spans, reinforced concrete is a better option as
145   the volume of stone masonry becomes heavier. Capacity building of local artisans and contractors
146   is another challenge to consider, as lack of expertise may be costly to replace. To this effect,
147   industrialised countries have opted to use pre-stressed concrete rather than investing money on
148   expert masons and casual labourers. In this framework, the stone arch technique for construction of
149   bridges is nowadays less employed or it has been abandoned [26].

150

151   3.1   Structural issues in masonry arch bridges

152   Main failures in historical arch bridges relate to the development of a mechanism chain with
153   formation of hinges, by sliding, or by a combination of these. Compression strength in models

accounting for these failures is not relevant. However, the masonry compression strength must be considered in two other instances, i.e., i) looking at the developing hinges where maximum compression forces are reached, and ii) considering arch bridges under maximum equal load. Maximum equal load can be reached by widening the road lane and therefore increasing the dead load of the bridge.

Structural defects can be normally related to four main factors, i.e., (i) construction, (ii) long-term loading, (iii) transient loading and (iv) the environment [25]. A combination of defects deriving from the contribution of all the above factors is usually verified in existing masonry bridges (Figure 2). It is also worth noting that modern traffic loads, heavier than in the past, could affect seriously the structural integrity of older bridges. On the contrary, well-maintained masonry arches not subject to heavy loads are probably among the most durable constructions.
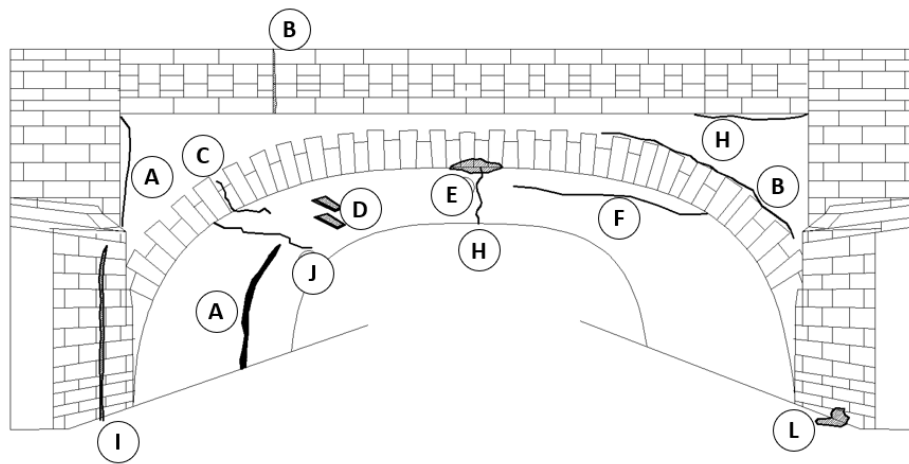
Fig 2 Most frequent damage types and location in arch bridges. A) cracks in the abutment joint or pier with arch; B) cracks in spandrel beam and parapet wall; C) cracks in corners; D) loosening of voussoirs; E) detachment at the arch key; F) longitudinal cracks; G) disconnection of the arch ring; H) opening of the spandrel beam; I) opening at the abutment wall; J) crosswise cracking; K) cracking at the arch key; L) deposits.

4   Assessment Methods for Masonry Arch Bridges

Several methods with different levels of complexity have been developed for prediction of in-service behaviour and load-carrying capacity of masonry arch bridges. These range from expeditious procedures based on empirical rules, to limit-state-analysis-based approaches [28], up to the most advanced non-linear computational formulations (e.g., finite-element and discrete-element methods).

According to Lourenço [29], selection of the most appropriate method depends on several factors. It is worth to mention, amongst others: (i) the structure under analysis; (ii) the desired level of accuracy; (iii) knowledge of material properties and experimental data available; (iv) financial resources; (v) time requirements and experience of the analyst. As a general recommendation, the best approach must guarantee a trade-off between amount of input information, overall fitting to different scenarios and viability of the outputs.

184 Three main classes of methodologies for structural analysis of masonry arch bridges and assessment
185 of load-carrying capacity can be identified [30]: (i) semi-empirical models, (ii) equilibrium-based
186 models and (iii) numerical models. To this effect, it worth mentioning that use of non-linear
187 numerical models (e.g., finite-element methods) is capable to provide a realistic simulation of the
188 structural behaviour of masonry arch bridges through advanced computational tools via non-linear
189 models. Within this framework, the provision of significant input data is a major task in numerical
190 modelling, regardless of the complexity of the numerical model. Therefore, the continuous
191 monitoring of historical masonry structures and collection of reliable information by advanced
192 monitoring techniques is crucial to ensure an effective structural assessment.

193

194 4.1   Inspection and monitoring techniques for the investigation of masonry arch bridges

195 *4.1.1   Destructive testing methods*

196 As well as the information on the geometric parameters of a bridge, numerical models require data
197 about material properties. Information are often collected from test specimens, taken from the
198 original structure [31]. To this purpose, destructive tests can be applied to samples and natural-scale
199 structural elements, leading to permanent damage. Their use is more constrained or not possible in
200 case of historical bridges. Semi-destructive tests are also performed with a lower intrusiveness in the
201 structure or material under investigation. Nevertheless, these methods cause a local loss of
202 functional properties and require repairing of the structure at the end of the testing process [32].
203 Main destructive testing methods used for the monitoring of masonry bridges are summarised in
204 Tab. 1.

205

206 **Table 1** Main destructive testing methods used for the monitoring of masonry bridges.

Method	Description	References
Core Drilling	Scope of this method is to extract material and provide geometrical information on the internal structure of the bridge. Cores are then visually analysed in order to collect information about layer thickness, and hollow sections, amongst others.	Proske and val Gelder [31] Berndt and Schone [33]
Flat-Jack Testing	Release of a stress in a small area of a structure by a plane cut perpendicular to its surface. The pressure is increased until the point of non-linearity is identified in the load-strain curve. A wide range of information can be estimated for structural assessment of old masonry buildings, including the masonry stress state, compression strength and the elastic modulus.	Vicente et al. [34] Bindia and Tiraboschi [35]

207

208 *4.1.2   Non-destructive testing methods*

209 Non-destructive testing is a multi-disciplinary scientific area concerning the evaluation, inspection,
210 testing and characterisation of materials and structures through methods that do not significantly
211 alter the original properties and arrangement of materials or structures [36]. There exist several types
212 of NDT techniques (Tab. 2) relying on different theoretical principles, and producing different sets
213 of outputs/information in regard to the physical properties of a structure [37]. NDT methods allow
214 for a non-intrusive and detailed survey of civil engineering infrastructures. To this effect, they have

become popular in the health monitoring of infrastructure heritage assets, where non-intrusiveness
to the structure is a key requirement [38].

Table 2 Main non-destructive testing methods used for the monitoring of masonry bridges.

Method	Description	References
Sonic transmission	Direct transmission involves the passing of a compressional wave through the thickness of the wall (or the structure) under investigation. The velocity magnitudes may be plotted in a contour map format. This allows a fast evaluation of the relative conditions of the masonry walls or an evaluation of the internal fabric of a structure, such as a masonry arch bridge.	AA.VV. [39] McCann and Forde [37]
Sonic tomography	This technique is an improvement of the sonic transmission test method as tests are performed along non-perpendicular paths to the wall surface as well as in a direct mode.	Colla [36] Williamson [40]
Seismic reflection	The initiation and reception of the sonic wave are both performed on the same face of the masonry such as in the case of the indirect transmission mode. The stress wave recorded is the direct stress wave reflected from any internal flaw or the rear face of the structure investigated.	McCann and Forde [37]
Impact-echo system	A stress pulse is introduced into a test object by mechanical impact on the surface. The pulse propagates into the object along spherical wave-fronts as compression or shear waves, or P- and S-waves. Arrival of reflected waves (or echoes) at the surface where impact was generated produces displacements that are measured by a receiving transducer and recorded by a data acquisition system.	AA. VV. [39]
Electrical impedance tomography	The method allows a 3D imaging of the dampness distribution in a brick wall by measuring its electrical properties.	Biernat et al. [41] Hola et al. [42]
Electrical resistivity measurements	The distribution of conductivity is determined through repeated measurements (for different configurations of the excitation probes) of potentials on the surface of the masonry.	Fauchard et al. [43] Bungey et al. [44]
Ground penetrating radar	The energy reflected by the dielectric discontinuities within the subsurface is recorded by means of a receiving antenna and it is subsequently processed and displayed through a display unit.	Benedetto and Pajewski, [45] Daniels, [46]
Infrared thermography	This technique is based on a process in which heat at any temperature is converted into a thermal image using specialised scanning cameras.	Solla et al. [47] Orban et al. [48]
Radiography	Very short wavelength electromagnetic radiations penetrate through solid media, being partially absorbed by the medium. The radiation passing through the material can be detected, recorded and monitored by electronic sensing equipment.	McCann and Forde [37]
Laser scanner	Laser scanner, also referred to as Light Detection And Ranging (LiDAR), is used for 3D data acquisition of both topographic and close-range objects. The equipment allows an automated dense sampling of the object surface within a short time range.	Lubowiecka et al. [49] Riveiro et al. [50]
Aiborne DinSAR	The airborne interferometric SAR system can detect ground displacements and motions due to natural hazard-events (i.e. earthquakes, landslides) providing high operational flexibility. Flexibility on diversifying directions of the flight-trajectory during the acquisition stage can overcome some of the limitations of satellite acquisitions, e.g. the detection of deformations along the North-South direction.	Perna et al. [51] Perna et al. [52] Perna et al. [53]
Unmanned Aerial vehicles	Unmanned Aerial Vehicles (UAVs) are flexible observation platforms suitable to cover inaccessible areas on demand. Research is focussing on the development of miniaturised sensing technologies complying with UAV payload constrains and capable of providing high-resolution images.	Rosen et al. [54]
Interferometric SAR	SAR system is an active satellite system that provides electromagnetic images of the Earth's surface by emitting electromagnetic pulses at frequencies ranging between 0.23 GHz and 40 GHz. The basic principle of InSAR relies on the phase comparison between multiple SAR images of the same investigated area collected at different time periods with similar looking angles from space.	Ferretti et al. [55] Colesanti et al. [56]

219

For the purpose of this paper, GPR and InSAR techniques are described in more details in the following subsections. For a deeper analysis of advantages and limitations of these techniques, readers are suggested to refer to Bianchini Ciampoli et al. [18].

223

4.1.2.1   Ground Penetrating Radar

The basic principles of GPR are well-established [57]. A transmitting antenna emits an electromagnetic (EM) pulse into the ground which is partly reflected when a target with different dielectric properties is encountered, and partly transmitted to deeper layers. The energy reflected from discontinuities in impedance is received by means of a receiving antenna and is subsequently processed and displayed by means of a display unit. If the transmitting and receiving antennas are moved at a constant speed along a linear path, a cross-sectional image of the material can be generated. Alternatively, if scans are collected in a regular grid pattern, a three-dimensional image of the target can be produced.

After the data acquisition stage, GPR datasets can be edited and several processing techniques can be applied in order to produce a clearer image for data interpretation and evaluation purposes. Preliminary processing steps are the application of temporal and spatial filtering and the use of time gain adjustments of signals recorded [58,59].

GPR has been successfully used to monitor bridge decks within the context of identification, assessment and health monitoring of rebars, rebar cover length, depth of cracks, settlements, ingress of moisture and delamination, layers of materials, cavities, location of rebars and other structural features (beams and columns) as well as bridge abutments (leakage, cracks and settlements) [49,60-65]. GPR is one of the most recommended NDT methods for use in masonry arch bridges in view of its rapidity in data collection, high accuracy and penetration depths as well as the provision of an overall qualitative internal image [37]. GPR has also proven potential at providing information about the hidden geometry [66], bridge foundation detailing [67], ring stone conditions [68], moisture content, fills conditions and asphalt cracking [62]. Usually, high-frequency antennas above 1 GHz are used to achieve the resolution for detection of shallow targets within the structure [69]. In some instances, such as the evaluation of the internal structure of a masonry arch bridge or a harbour dock wall, a higher penetration of the electromagnetic energy is required and lower frequency antennas in the range 100÷500 MHz must be used.

Lubowiecka et al. [49] used the GPR technique for the estimation of homogeneity and heterogeneity features in a bridge structure. In order to model the structural behaviour of the bridge, a finite element-based structural model was defined by integrating GPR and laser scanner data. In this regard, Saarenketo [70] argued that, due to the complexity of information involved in a bridge survey, stand-alone use of GPR cannot provide a comprehensive framework for structural health monitoring purposes. However, it is recommended for initial mapping and subsurface target location. GPR was also coupled with laser scanner by Solla et al. [66] to assess historical masonry arch bridges. The technique has proven good potential in providing valuable information about hidden geometric features of the bridge, and the integration with laser scanner data allowed to create finite-difference time-domain (FDTD) models of the bridge. Solla et al. [66] used GPR to survey

260 several stone arch bridges located in Spain. Results revealed previously unknown geometrical data
261 and hidden internal characteristics of the bridges, including the presence of internal voids, ancient
262 arches and restorations. Use of numerical modelling was done in order to identify the effects of
263 noise-related factors to the GPR signal and extract more viable information from the GPR datasets.
264 Numerical modelling was also used by Diamanti et al. [68] to simulate GPR testing scenarios and
265 investigate ring separation effects in brick masonry arch bridges. Outcomes have proven a good
266 correlation between numerical and actual GPR experiments. Conde et al. [71] presented a
267 multidisciplinary approach for the structural assessment of masonry arch bridges, carrying out a
268 comprehensive field survey fully based on the use of NDT techniques. To this purpose, laser
269 scanning, GPR, sonic tests and ambient vibration testing were integrated. Results demonstrated a
270 significant impact of the tensile nonlinear properties of masonry and the importance of fill materials
271 on the structural integrity of arch bridges. Moreover, advantages of using a three-dimensional
272 modelling approach were also pointed out, as critical transverse effects in the response of the
273 structure were successfully identified. Similarly, Bergamo et al. [72] combined GPR data with
274 information collected from destructive and non-destructive testing methods for the evaluation of
275 historical masonry arch bridges. The study investigated advantages of each technique in order to
276 identify an optimised in-situ testing procedure. The authors found the integration between GPR and
277 the thermographic analysis as effective for detection of moisture, discontinuities and non-
278 homogeneities in bridges.

279

280 *4.1.2.2   InSAR for bridge monitoring*

281 InSAR is a well-acknowledged remote sensing technique which has been applied since 1980s to
282 evaluate the deformation of the Earth's surface [16], for geophysical monitoring of natural hazards,
283 e.g., earthquakes [73], ice motion [74], volcanism [75], landslides [76], and in subsidence and
284 structural stability assessments. The SAR system is an active satellite system that provides
285 electromagnetic images of the Earth's surface by emitting electromagnetic pulses at frequencies
286 ranging between 0.23 GHz and 40 GHz. The received component of the spread field caused by the
287 scattering phenomena on the ground is therefore analysed in order to provide the final output.

288 A unique advantage of SAR satellites is the availability of new datasets of SAR images collected at
289 every satellite orbit around the Earth. The time elapsed between two consecutive observations of the
290 same area, known as the revisiting period, depends on the satellite's orbit and can reach up to a one
291 day-period.

292 The basic principle of InSAR relies upon the phase comparison between multiple SAR images of the
293 same investigated area collected at different time frames with similar looking angles from the space
294 [77-80]. The phase difference is proportional to the surface deformation occurring at the time interval
295 between the acquisition of two consecutive images. However, it is also affected by the contribution
296 of topographic and atmospheric factors. Differential InSAR (DInSAR) refers to the interferometric
297 analysis of a pair of SAR images to identify and detect displacements on the Earth surface by
298 removing the topographic contribution through a Digital Elevation Model (DEM). Figure 3 shows
299 the relationship between the ground displacement measured along the satellite Line of Sight (LOS)
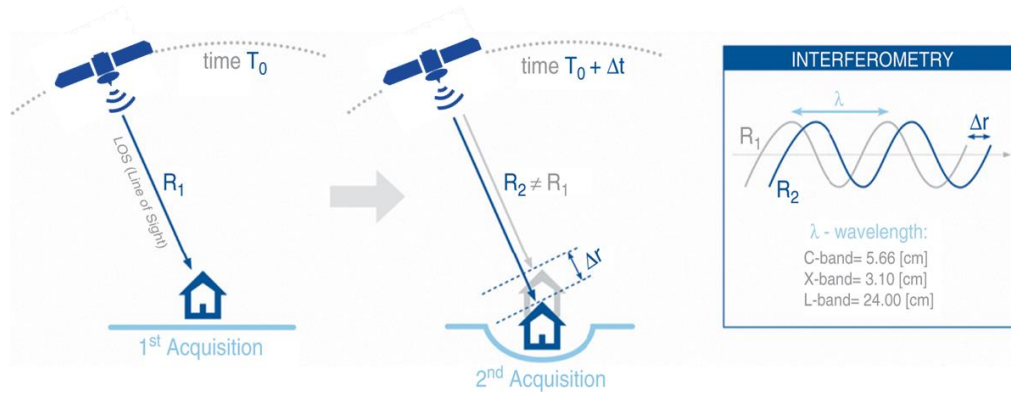300 and the signal phase shift.

Fig. 3 Main working principles of the DInSAR technique.

Following an extensive application of the DInSAR technology during the 90s, the atmospheric contribution to the signal phase was identified as significant and affecting the quality of data collected. In addition, the DInSAR allows for the detection of the phase difference only between two SAR images. These limitations were overcome by the development of Permanent Scatterers Interferometry (PSI) techniques, such as the PSInSAR [14] and the Small Baseline Subset [15,81].

These techniques are based on the statistical processing of multiple SAR images and a multi-temporal interferogram analysis, for extracting long-term high phase stability benchmarks of coherent PS point targets, namely Persistent Scatterers (PS) [14,55]. This allows to identify and remove atmospheric-related noise and improve the accuracy of deformation measurements.

The main innovation of the PSI approach is in the possibility to analyse specific points on the ground surface, i.e., the PS, and monitor the historical trend of their deformations. PS are characterised by a stable amplitude and a coherent phase across all set of images in a dataset [14,55]. PS are usually fixed features on the ground such as exposed rocks, manmade structures and infrastructures (e.g., railways, buildings, bridges, transmission towers), rocky outcrops, and any other permanent feature that reflects a stable signal back to the satellite. The SBAS approach [81,82] is suitable to provide dense coverage and higher precision for spatially smooth occurrences where no-point targets might be identified but large, correlated displacements occur over natural targets. Recently applications in Urban-cities were presented by [83] and [84] that confirm the innovativeness of the matters.

Finally, recent innovative results were obtained also using UAVS [52] and Airborne DInSAR [51] which starting from the pioneering experiments of the last decade, is today affirming as a disruptive technology through the use of drones and UAVs.

The PSI technique, such as the PS-InSAR by Ferretti et al. [14] and Ferretti et al. [55] is more effective for high-spatial resolution occurrences, especially in case of very stable reflectors (i.e. man-made, infrastructures monitoring, bridges) that might have independent displacements compared to the surrounding areas [14,55]. The PSI technique was applied for the purpose of this research, and the results are presented in Section 5.2.2.

The PSI technique works by the application of the following steps [55,57,85]:

   i. a statistical analysis of the amplitudes of the electromagnetic returns is developed on a pixel-by-pixel base to compute an index of stability over time for each pixel;
   ii. identification of permanent scatterer candidates (PSC). These are pixels with a value of stability index that exceeds a fixed threshold;

iii.   computation of the interferometric phase $\Delta\varphi i$ for any PSC, at any i^{th} interferogram;

iv.   identification and removal of the atmospheric phase contributions, orbital and noise-related effects from the interferometric phase.

As a result of the above process, stable reflectors, i.e. the PS, can be identified over the inspected area. This allows surface displacements to be measured with a millimetre accuracy [14,86]. At the end of the process, displacement evolution trends can be generated for every PS, or an average velocity map can be produced to provide an overview of the average ground motion over the entire area of interest. Use of the PSI technique in the monitoring of bridges and transport infrastructures (such as roads and railways) has been presented in several research [17,87-90] proving the applicability of the method and the interest of the scientific community.

5   Case Study: the Aylesford Arch Bridge

The "Old Bridge" at Aylesford, Kent, UK is a multi-span bridge dating from around 1250 (Figure 4).

Fig. 4 Main features of the "Old Bridge" at Aylesford in Kent, UK. (a) side view of the bridge spans with details of the main central arch span width and (b) width of the carriageway.

The bridge is constructed of local "ragstone" with seven arches including a central segmental arch and six pointed and double-chamfered outer arches. The bridge width is about 4 m between the centres of the stone-coped parapet. The end arches are partly buried by the river bank. The stone piers have cutwaters on the upstream and downstream sides on rebuilt concrete foundations. On each side, are octagonal and triangular canted pedestrian refuges resting on buttresses over the piers. Below the bridge is a barge-bed constructed from large baulks of timber. The bridge underwent a major alteration in the early 1800s, when the two central arches were replaced by a single arch of 18m span, removing a pier to allow passage for larger river traffic.

The bridge traffic is closed to cars and motorbikes, although it remains in use for pedestrians, cyclists and horses. It is a scheduled ancient monument under the control of the English Heritage.

364   5.1   Equipment and surveying methodology

365   *5.1.1   GPR*

366 GPR data were collected using several systems (Figure 5). The high-frequency acquisitions were
367 carried out using the RIS Hi-BrigHT GPR antenna array manufactured by IDS GeoRadar (Part of
368 Hexagon) (Figure 5a). The system consists of two rows of eight double-polarised 2000 MHz antennas
369 with a spacing of 10 cm that allows scanning with a footprint 80cm wide.

370 The survey was divided into three scanning 'Zones' to ease the data management stage (Figure 6).
371 The bridge deck was surveyed collecting four equally-spaced longitudinal scans along the main axis
372 of the bridge (Figure 7). In view of the cross-polarised configuration of the RIS Hi-BrigHT system,
373 transversal scans (i.e., scans across the bridge width) were not collected. However, the cross-
374 polarisation feature allowed to provide reliable C-scan maps at different depths.

375
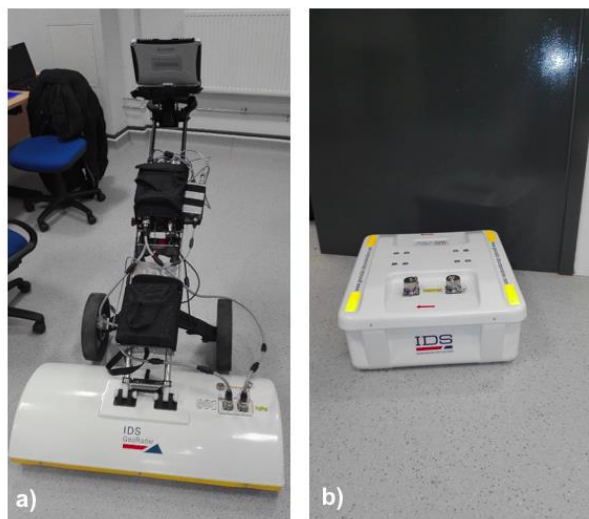
376

377 **Fig. 5** GPR antenna systems used for the investigation of the Aylesford bridge: the IDS Hi-BrigHT 2000 MHz
378 antenna system a) and the IDS RIS MF Hi-Mod system equipped with the TR Dual-F 200 MHz and 600 MHz
379 antenna b).

380
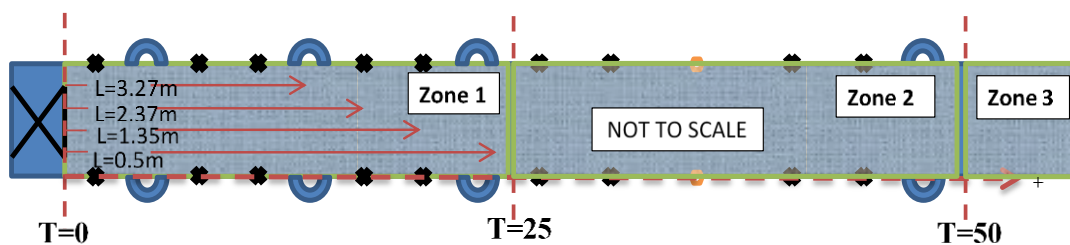
381

382 **Fig. 6** The "Old Bridge": drawing of the three survey zones.

383
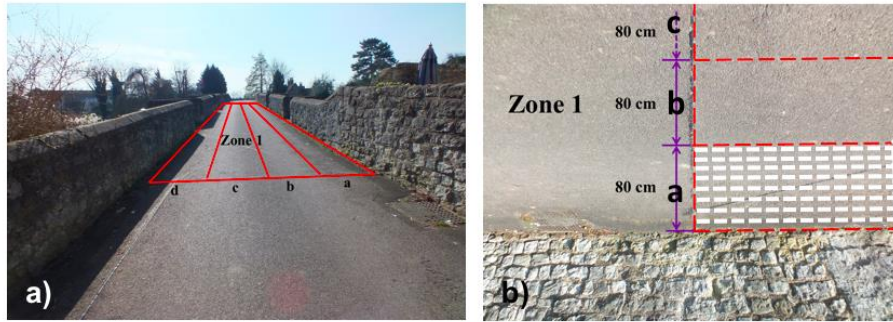
Fig. 7 Survey scheme of the "Old Bridge" followed using the 2000 MHz antenna system.

In addition to the above, identification of reinforcement bars from structural ties through the bridge structure was also carried out. To this purpose, four scans were performed using the TR Dual-F 200 MHz and 600 MHz antenna system (reference penetration depth of 1.5 m and 2.5 m, respectively) from the IDS RIS MF Hi-Mod (Figure 5b). The GPR apparatus contains an array of two antennas with frequencies optimised for underground utility detection. Same reference coordinates taken for the high-frequency GPR surveys as well as the same three areas were considered for this investigation (Figure 8). It worth noting that four main scanning lines (i.e., white arrows in Figure 8a) were collected across the width of the bridge at the central axis of the area covered by the RIS Hi-BrigHT antenna array.
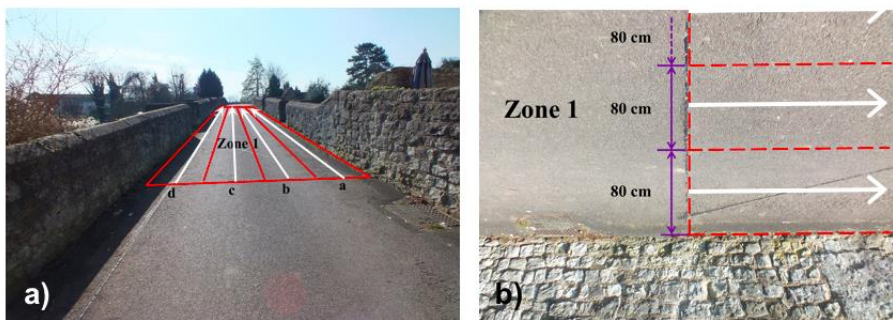
Fig. 8 Survey scheme of the "Old Bridge" followed using the 200 MHz and 600 MHz dual frequency antenna system: perspective view (a), and plan view (b).

5.1.2 SAR Imagery

Details of the dataset used for the interferometric analyses are listed in Tab. 3. At this stage of the research, a dataset of C-band SAR with a medium-range resolution accuracy was collected and processed to test the feasibility of the PSI application for the monitoring of the Area of Interest (AoI). The analysis of the area is expected to be detailed by processing higher resolution X-Band SAR data in a future stage of the research, in order to analyse the detected phenomena at a larger scale.

In this study, different single look complex (SLC) SAR images acquired in the interferometric wide swath (IW) mode from the Sentinel-1a satellites (Figure 9) were used and processed. The Sentinel1A mission is equipped with a C-SAR sensor with a medium-range resolution operating at C-band. The

sensor has a central frequency of 5.4 GHz, corresponding to a wavelength of 5.55 cm. The IW mode has a 250 km swath and a spatial resolution (single look) of 5 m in ground range and 20 m in azimuth. After the application of the multi-looking operation, the spatial resolution of every pixel is 20mx20m.
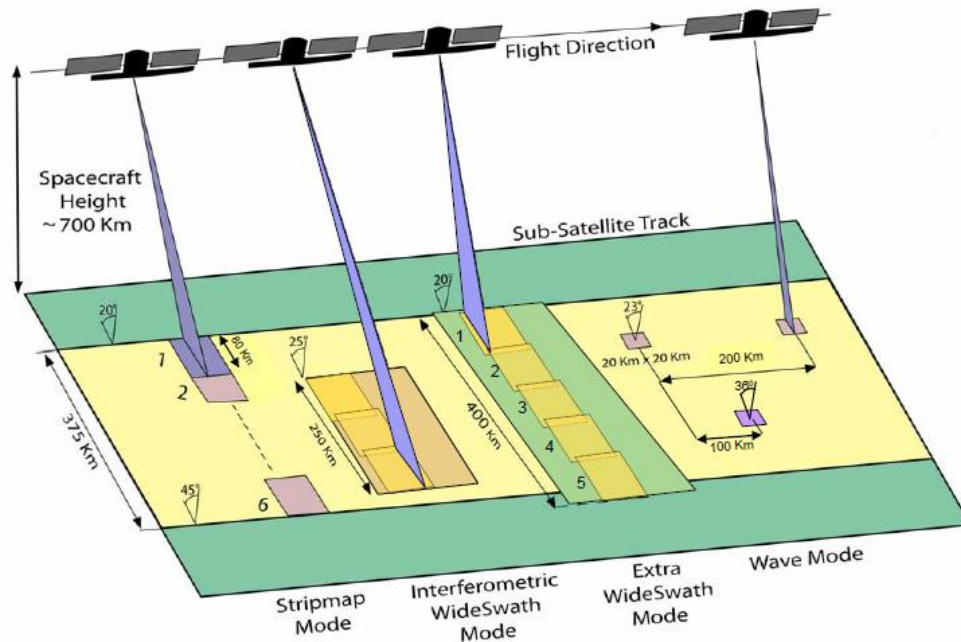
Fig. 9 SENTINEL-1 acquisition modes.

Table 3 Main information on the Sentinel 1A SAR imagery used.

Sensor	Data Ownership Rights	Frequency	Resolution	Number of Images	Revisit Time (Days)	Acquisition Time Range
Sentinel-1 A	The European Space Agency (ESA)	5.4 GHz	Centimetre	21	12	06/2015 ÷ 03/2017

The data used in this study were acquired in the period comprised between June 2015 and March 2017, and images were provided by the European Space Agency (ESA).

It worth noting that number of images in descending selected orbit (chosen for the selection of SAR images in ascending geometry) that covered the inspected area of interest were not enough for PSI processing purposes within the period of interest. Therefore, results achieved in this paper are exclusively referred to the ascending geometry.

5.2   Results

5.2.1   GPR investigations

Investigations carried out for the assessment of the entity of existing areas of surface damage with the 2000 MHz antenna system showed evidence of surface reinstatement at all the three identified

zones. This was allowed by the combined analysis of B-scan and C-scan maps from the data
collected. An example of identification of the sources of surface damage using the above approach
is provided in Figure 10. Depth-to-time conversion was achieved by assuming a wave propagation
velocity v of 10 cm/ns, i.e., an average dielectric permittivity ε_r in the multi-layered structure of 9.
This is in line with values indicated in literature review for materials composing the investigated
bridge subsurface structure [46].
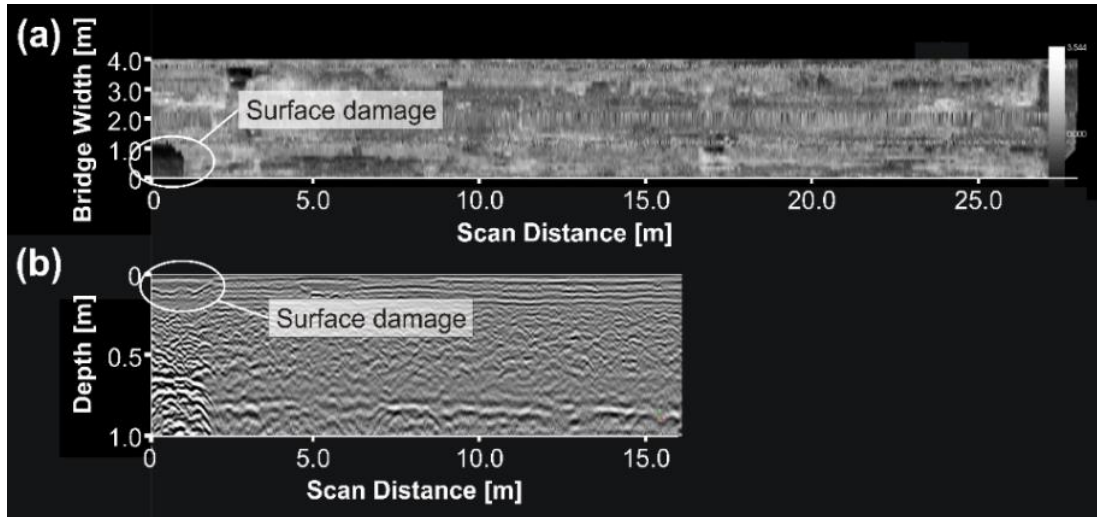
Fig. 10 Surface reinstatement over identified surface damages in Zone 3 from (a) a C-scan (5 cm deep) and (b)
a B-scan view.

Structural detailing has proven a second layer of base material placed beneath the asphalt layer and
directly on top of the stonework. This was likely arranged to avoid irregularities in the stone surface
and to provide a more uniform distribution of loads at the bottom of the structure.

Overall, the survey carried out with the 2000 MHz antenna system identified the total depth of the
bridge deck above the historic stonework to be variable across the bridge length, with the minimum
depth being at the centre of the widest arch. Figure 11 shows some of the most representative B-
scans collected over the three zones.
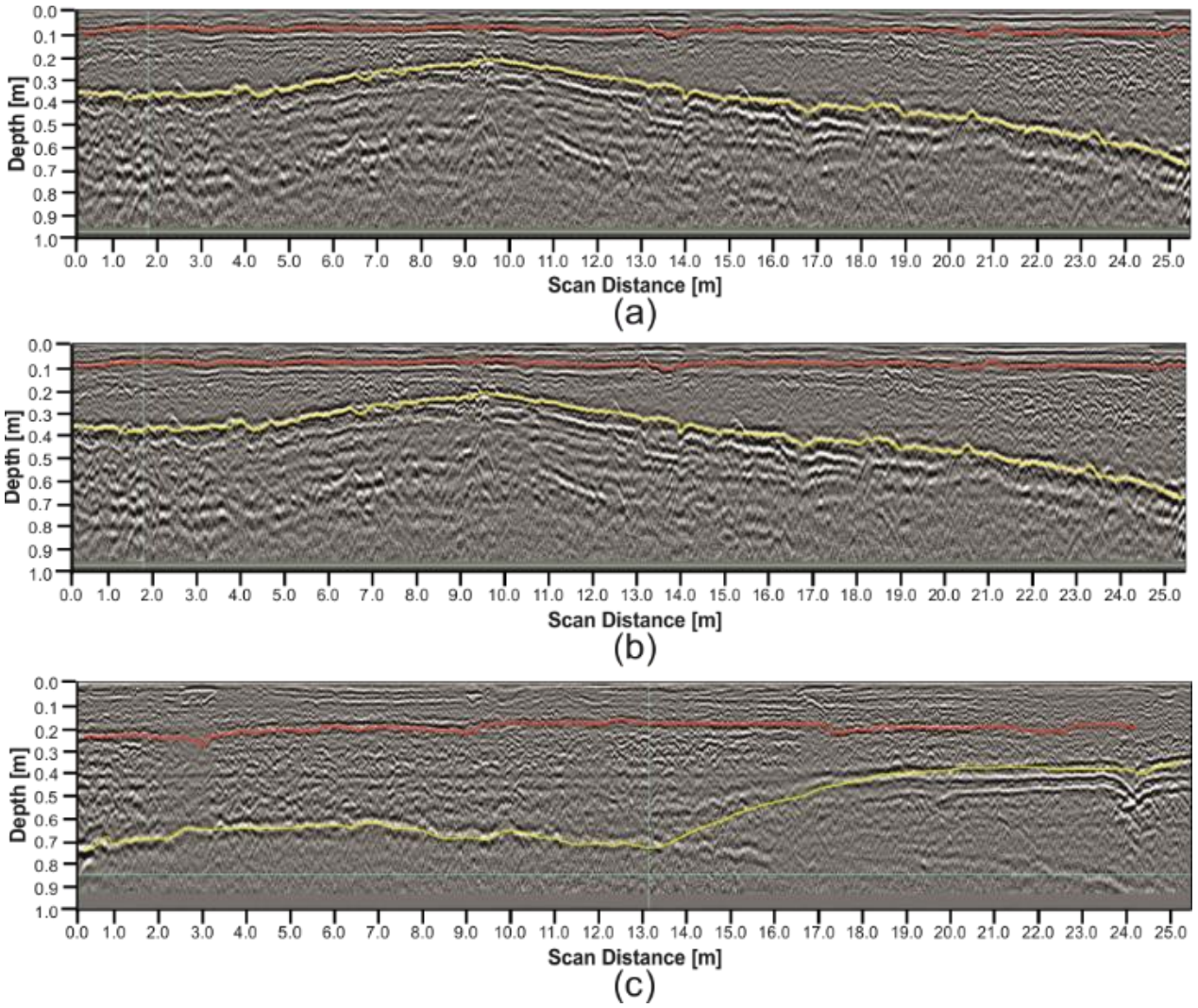
Fig. 11 B-scans collected at the three zones from scan lines within the 2000 MHz antenna system array. Top contour line (red): interface between the asphalt (top) and the base (bottom) layers; bottom contour line (yellow): interface between the base layer (top) and the historic stonework (bottom). Zone 1 (a), zone 2 (b) and zone 3 (c).

In general, it is possible to estimate the thickness h_{ij} of the ith layered medium at the jth zone using information on the velocity of propagation of the EM signal in the medium v ($v = 10$ cm/ns, assumed as a constant average velocity across the multi-layered structural configuration of the bridge deck) and the time delay Δt_{ij} between two consecutive reflection pulses in a GPR signal (i.e., reflections from the top to the bottom interfaces of the ith layer at the jth zone). These three variables are related each other's by the following expression:

$$v = 2h_{ij} / \Delta t_{ij} \qquad (1)$$

The thickness values h_{ij} estimated from the scan lines of the antenna array have been averaged across the width of the carriageway in order to obtain average thickness values $\bar{h}_{ij}$ at the three zones.

461 With the purpose of providing an overview of i) the thickness of the asphalt layer and ii) the total
462 depth of the bridge deck above the historic stonework, their average thickness value $\bar{h}_{ij}$ at each of
463 the three zones and the corresponding standard deviation σ_{ij} were calculated (Figures 12 and 13).

464

	Asphalt Layer Thickness [cm] / (σ) [cm]
☐ Zone 1	7 (1)
☐ Zone 2	7 (2)
■ Zone 3	10 (6)
▨ Full Length	8 (4)
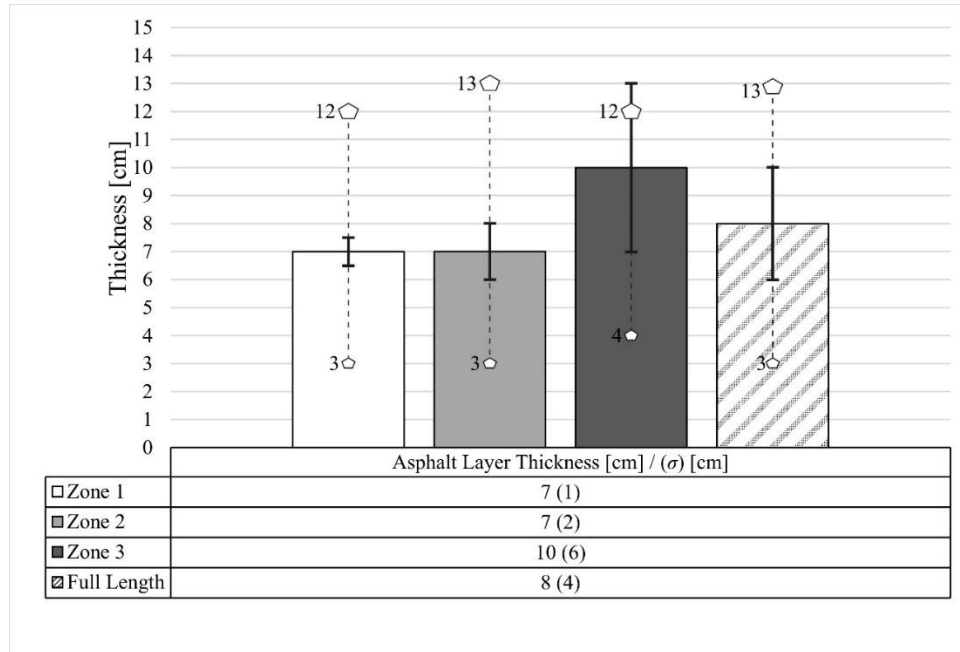
465

466 **Fig. 12** Thickness of the asphalt layer at the three zones investigated. Solid lines on each bar graph represent
467 the standard deviation of the values. Dashed lines stand for the range of values between maximum and
468 minimum values observed within the dataset of each zone.

469

470 Thickness values of the asphalt layer are not uniform and vary from 3 cm to 12 cm in Zone 1, 3÷13
471 cm in Zone 2 and 4÷12 cm in Zone 3 (Figure 12). The average thickness is 8 cm. In regard to the range
472 between minimum and maximum layer thickness over the three zones, the smallest variation (both
473 standard deviation σ_{min} and $\Delta h_{min \div MAX}$) was collected in Zone 1. On the contrary, the largest
474 variation in terms of $\Delta h_{min \div MAX}$ was collected in Zone 2. Zone 3 turned out to be the area with the
475 largest variability of the asphalt layer thickness, according to the highest value of observed standard
476 deviation (σ_{MAX} = 6 cm).

477 Figure 13 reports the bar graphs of the average value of the total depth of the bridge deck above the
478 historic stonework at each of the three zones and corresponding standard deviation.

479
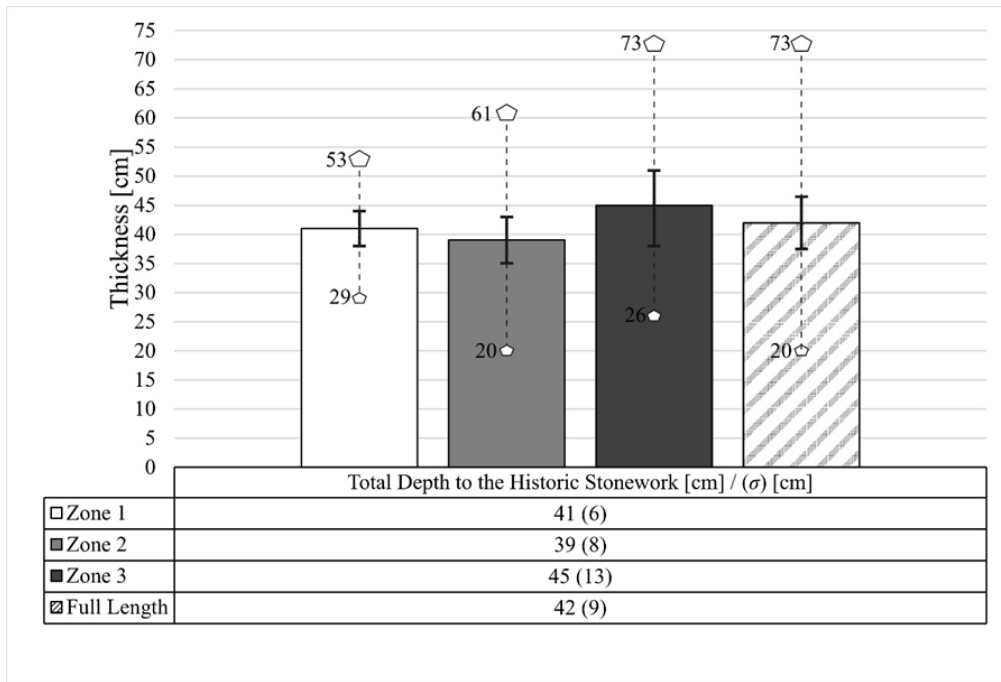
Fig. 13 Total depth of the bridge deck above the historic stonework at the three zones investigated. Solid line on each bar graph represents the standard deviation of the values. Dashed lines stand for the range between maximum and minimum values observed within the dataset of each zone.

Data analysis has demonstrated that total depth of the bridge deck above the historic stonework is not uniform and varies across the surface of the bridge. The minimum value is oserved in Zone 2, whereas the maximum depth is in Zone 3; the average depth is 42 cm. Similarly to the case of the asphalt layer thickness, the smallest variation in terms of both standard deviation and $\Delta h_{min \div MAX}$ (i.e., the range between minimum and maximum values of total depth of the bridge deck above the historic stonework within the concerning zone/dataset) was collected in Zone 1. In this regard, Zone 3 confirms to be the area with the largest variability ($\Delta h_{min \div MAX}$ = 53 cm) and standard deviation (σ = 13 cm).

It worth noting that reliability of data for depths beyond 40 cm could be lower compared to shallow depths, due to the limited penetration of the high-frequency antenna system. In addition, the considerable variations observed for the asphalt layer thickness and the total depth of the bridge deck above the historic stonework are likely related to the reconstruction underwent by the bridge in the past (i.e., replacement of the two central arches) and the large areas of resurfacing identified (Figure 14).
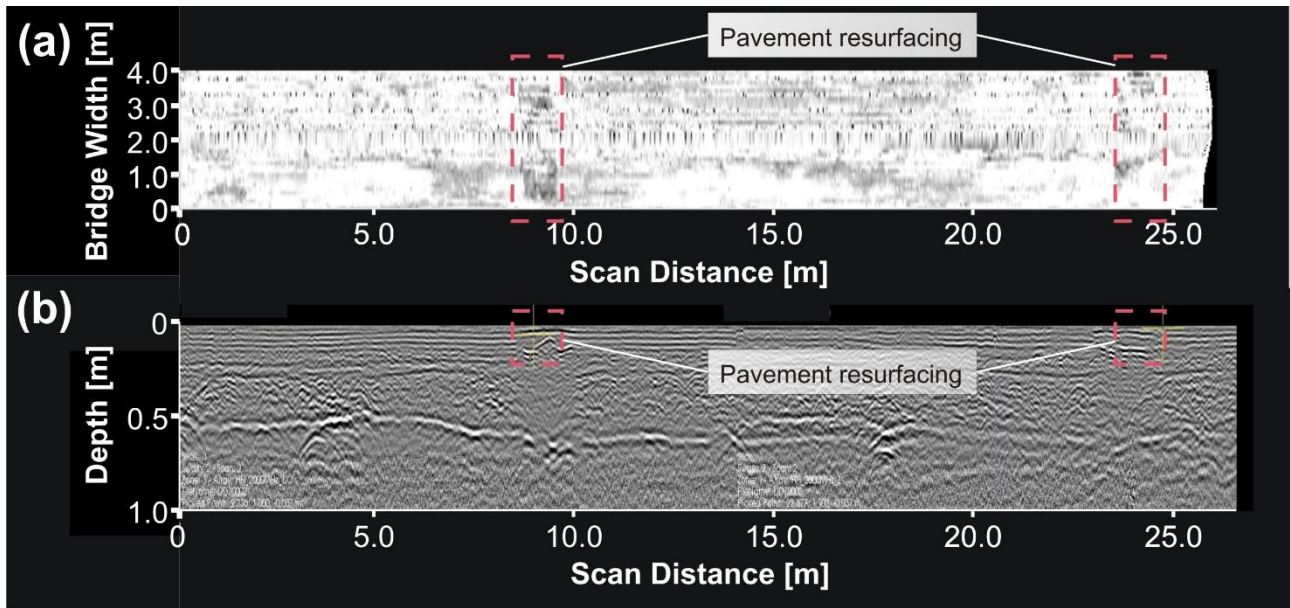
Fig. 14 Evidence of pavement resurfacing across the whole width of the carriageway identified in Zone 1 from (a) a C-scan (4 cm depth) and (b) a B-scan view.

In regard to the use of the low-frequency antenna system, the 200 MHz and 600 MHz dual frequency GPR was able to identify and locate the structural tie bars (Figure 15). Where location of these targets was unclear, cross-matching with information collected from manual measurements and laser scanner equipment were considered for the interpretation of the GPR data. This allowed to identify hyperbolic reflection features to relate uniquely to the position of the structural ties, in case of weak or multiple reflection patterns. More information about surveying methods, data processing and presentation of data from the application of these techniques can be found in Alani et al. (2017). Targets were positively identified within Zone 1 (5 tie bars – Figure 15) and Zone 2 (4 tie bars). No structural tie bars were found in Zone 3.
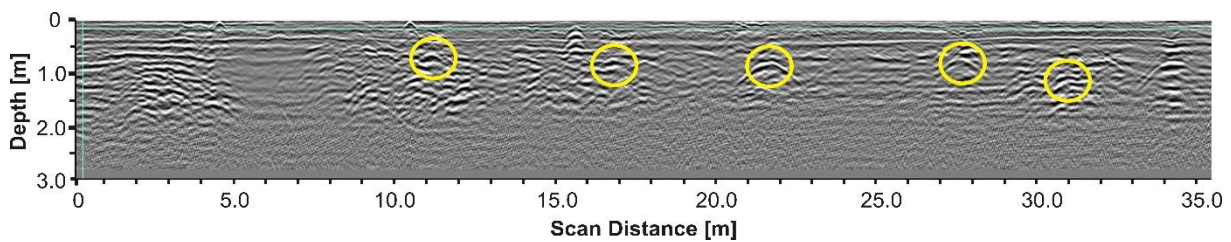
Fig. 15 Structural tie bars identified in Zone 1 using the 600 MHz central frequency antenna (IDS RIS MF Hi-Mod GPR system).

5.2.2   Persistent Scatterers Interferometry (PSI) analyses

Results from the application of the PS-InSAR technique to the acquired datasets are reported in Figure 16. Use of this technique has proven effective in identifying a set of 11 Permanent Scatterers in the vicinity of the bridge.

521 The multi-temporal InSAR image processing workflow used to identify PS coherent targets and
522 estimate their annual average motion velocity and temporal history of displacements along the
523 satellite LOS direction, was developed according to the PS Interferometric Stacking Module. This
524 tool is available in the software SARscape integrated in Envi [91-93], under the license of the Eohops
525 Project MOBI approved by ESA (European Space Agency). Furthermore, a SRTM v3 DEM (Digital
526 Elevation Model) was collected and implemented into the interferometric process [94,95] in order to
527 identify and subtract the phase-related parameters linked with the topography.

528 Outputs were exported into a GIS software and the PSs were displayed as a function of the average
529 annual motion velocities.
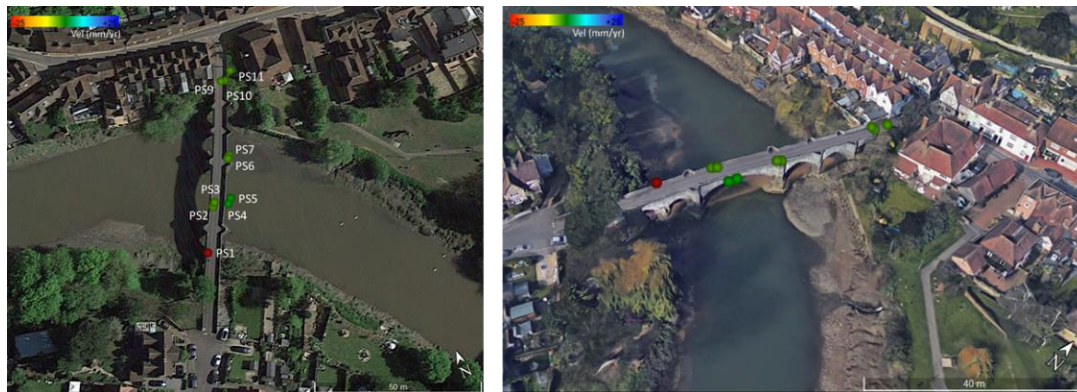
530

531 **Fig. 16** Plan view and 3D view of the PSs on the bridge.

532

533 Amongst the cloud of PSs obtained from the interferometric analysis, a subset of eleven PSs with a
534 temporal coherence from 0.65 to 0.80 have been identified as significant for bridge monitoring
535 purposes. Identified points have a temporal coherence ranging between 0.65 and 0.80. This implies
536 that use of a medium-resolution cell on the ground allowed to detect numerous points on the area
537 with a stable intensity. These spots were identified as PSs. In this regard, it is fair to comment that
538 these spots do not provide point information at the position of single structural elements of the
539 bridge. However, they constitute an essential information within the resolution area covered by the
540 satellite image with a huge potential for integration with other ground-based techniques.

541 As an example, a downward displacement is detected at the position of permanent scatterer PS1
542 (coherence of 0.64). Considering a pixel resolution on the ground of 20m × 20m, and the low
543 backscatter effect exerted by the river crossing the bridge, it is reasonable to relate this occurrence to
544 the bridge. The deformation velocity of the PS1 point is around -1.45 cm/year in the LOS direction.
545 Figure 17 shows the displacement history of point PS1 observed on the Aylesford Bridge within the
546 observation time frame.
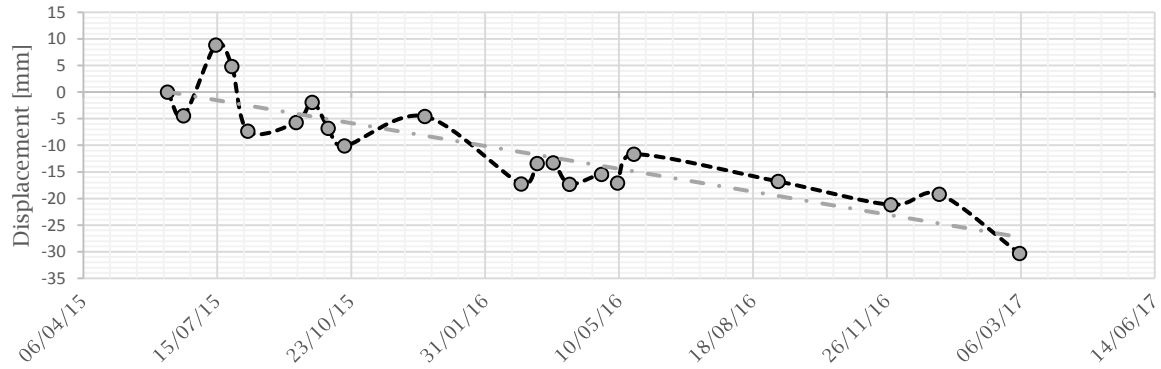
547

548   **Fig. 17** Displacement time series of point PS1 observed between June 2015 and March 2017.

549

550   Furthermore, various PSs are located nearby the spans and the stack of the bridge. Figure 18 is a 3D
551   view of concerning PSs (PS2, PS3, PS6, PS7) identified in these areas. It worth to emphasise that use
552   of medium-range resolution cells does not allow to relate the displacements to a specific structural
553   element on the bridge deck. Nevertheless, it allows to identify areas of major concerns and black
554   spots where maintenance activities could be potentially prioritised.
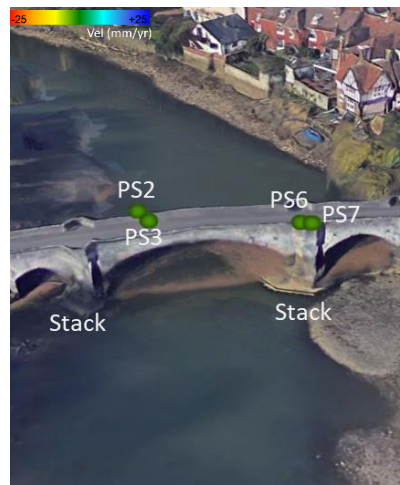
555

556   **Fig. 18** PSs located in proximity of the spans and the stack of the bridge.

557

558   From the observation of the displacement trends for the above set of PSs, it is possible to observe
559   seasonal effects on the upward and downward displacements of the scattering features over time.
560   In Figure 19, the displacement history of PS2 and PS7 is reported. It can be noticed an upward
561   displacement taking place in winter time for both the PSs, whereas downward displacements are
562   observed in late-springs and early summers.

563
564   (a)

565
566   (b)
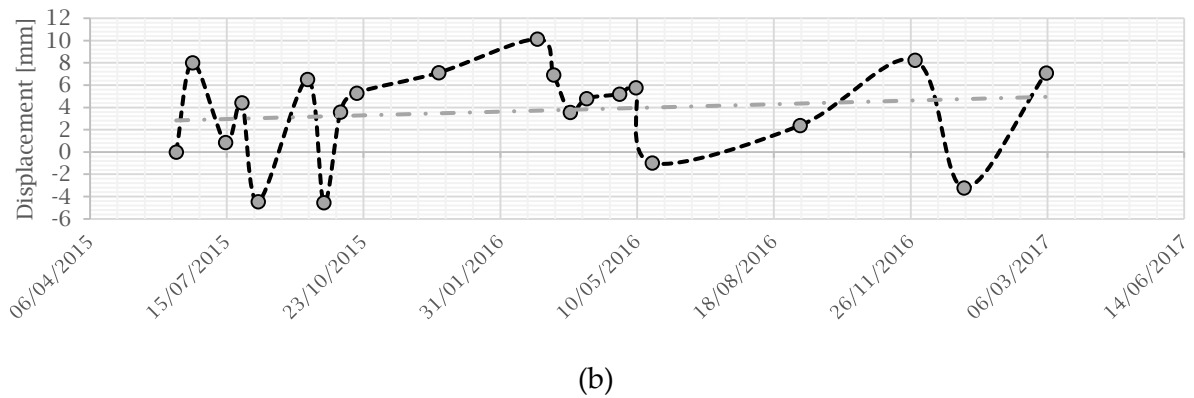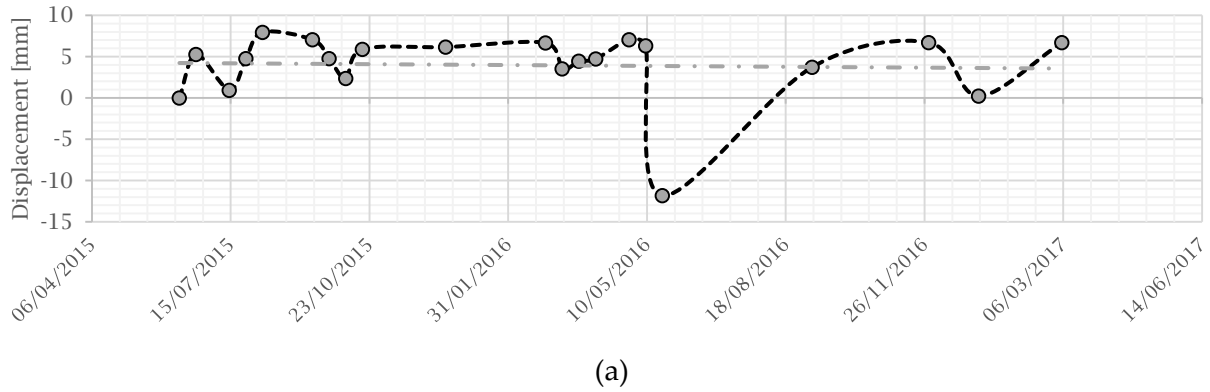
567   **Fig. 19** Displacement time series of points PS2 (a) and PS7 (b) observed between June 2015 and March 2017.
568   The point-dashed linear lines represent the average displacement trend for the concerning PS.

569

570   A detrending operation was applied to investigate potential cyclical (seasonal) trends of the
571   displacements. To this effect, a trend in a time series is usually referred to as a change in the mean
572   of a function over a certain observation time. Accordingly, following the application of a detrend
573   process to the data, it is possible to remove a time-related effect from a particular event (such as a
574   down-lift or an up-lift event) causing distorted interpretation of results. To this effect, a linear
575   regression (LR_i) of the temporal deformations was calculated for each ith PS and the following
576   equation was applied:

577                          $$PSp_i^*(t) = PSp_i(t) - LR_i(t)$$ (2)

578   where t is the observation time, PSp_i is the position of the ith PS referred to the position of a stable
579   point (displacement = 0) and PSp_i^* is the detrended behaviour.

580   Furthermore, a normalisation process of the data was applied in order to compare seasonal trends
581   at various PSs with different amplitudes of displacements.

582   The millimetre displacements are expressed with reference to a known stable PS (displacement = 0)
583   in the observation time. Specifically, various PSs with a similar trend of deformation were detected.
584   The output of this analysis is reported in Figure 20, where the normalised displacement is displayed
585   against the acquisition time within the observation period.

586
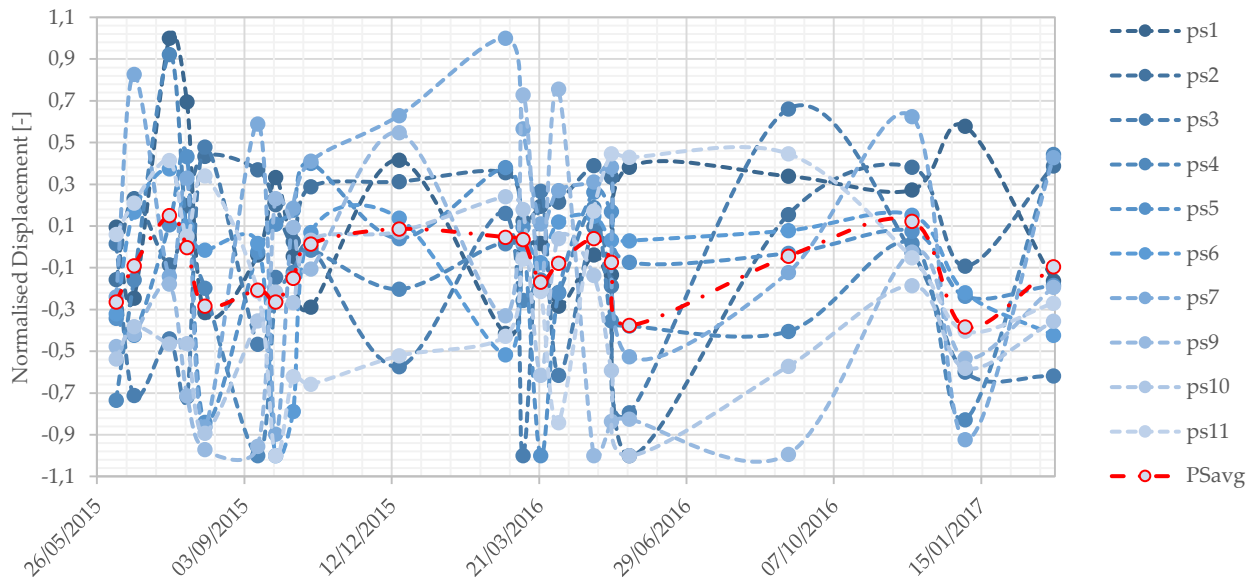
Fig. 20 Normalised detrended displacements for the identified set of 11 PSs observed between June 2015 and March 2017. The point-dashed (red) line represents the average displacement trend (PSavg).

589

The detrending and normalisation stages highlight an upward trend of displacements during late summer periods and a downward displacement trend during springs and falls.

The seasonal behaviours observed as a result of the PS analysis were compared to the hydrometric data of the concerning area. To this purpose, flood data of the Medway River were analysed from datasets by the UK National River Flow Archive (NRFA), hosted by the Centre for Ecology & Hydrology [96]. The archive is the main focal point for hydrometric data in the UK, providing stewardship of, and access to, daily, monthly and flood peak river flow data from over 1,500 gauging stations across the UK. The NRFA collates, quality controls, and archives hydrometric data from gauging station networks across the UK including the extensive networks operated by the Environment Agency (England), Natural Resources Wales and the Scottish Environment.

In more detail, data of the flood (m^3/s) collected from the two nearest downstream stations to the bridge location were used and analysed in this study:

- Station 40003 - Medway at Teston / East Farleigh (square marker in Figure 21)

- Station 40029 - Len at Lenside, tributary of the Medway River (round marker in Figure 21)

604
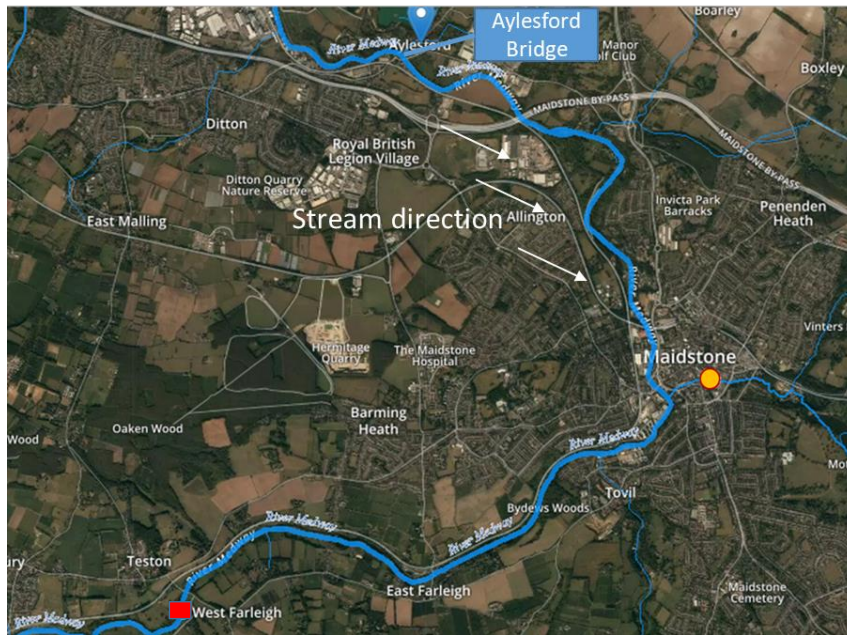
605 **Fig. 21** The two Stations considered for collection of the hydrometric data.

606

607 Possibility to analyse the hydrometric trend of the area since 1985 was available. In order to
608 investigate a potential correlation between hydrometric and displacement data and verify potential
609 delayed effects, a larger period of observation (i.e., from January 2015 to April 2017) was considered
610 compared to the time frame used in the PS analysis (i.e., from June 2015 to March 2017). The output
611 of the flood analysis is reported in Figure 22, where the normalised flow is plotted against the
612 acquisition time from stations 40029 and 40003.

613

614
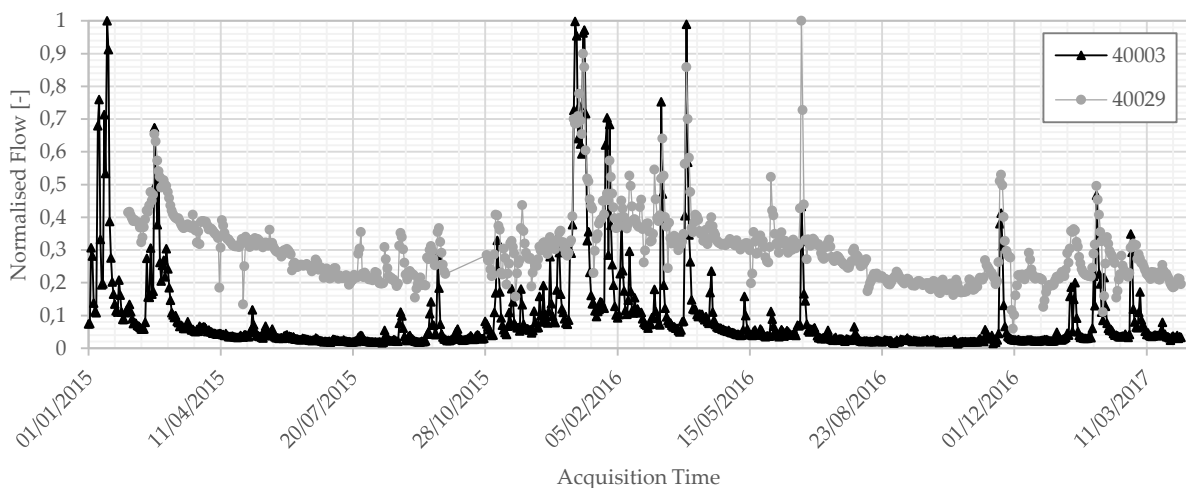
615 **Fig. 22** Normalised hydrometric flow data from stations 4003 (triangular markers) and 4029 (round markers).

616

617 A correlation between displacements identified by the InSAR analysis at the PS positions and the
618 flood trends recorded by the two stations is observed. More specifically, flood events occurred at

winter time periods in years 2016 and 2017 (arrows in Figure 23) are found to have a close trend to
the peaks of upward displacements on the bridge observation area.
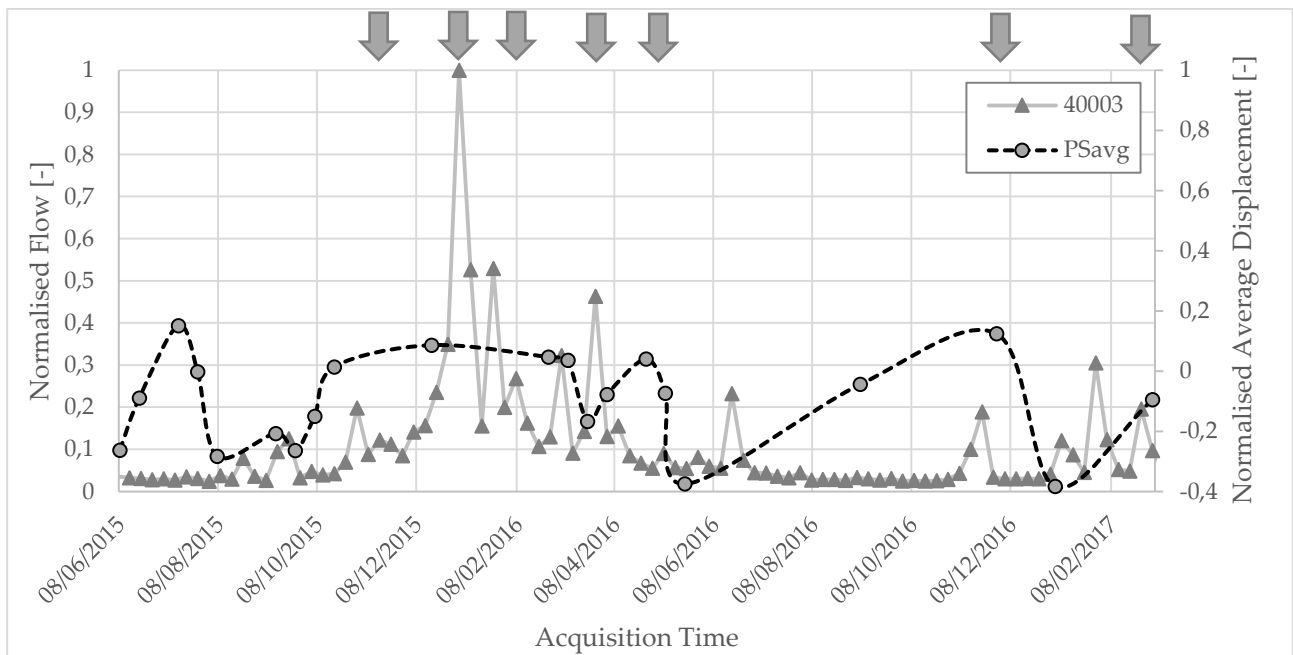
Fig. 23 Comparison between the average trend of identified PSs and the hydrometric trend (weekly average
– station 40003) observed between June 2015 and March 2017. Position of the arrows indicate flow peak
periods matching with the upward displacements of the bridge.

An interpretation for this behaviour is most likely on the upward hydrostatic pressure generated by
the swelling of the subgrade at the foundation level. This is in turn due to the period's rainfall and,
accordingly, to the hydraulic head of the Medway River. Although the limited resolution of the
dataset does not allow a detailed assessment of potential differential settlements for specific bridge
components, the general seasonal trend observed for the PSs in the bridge area indicates that the
whole structure is subject to cyclical patterns of upward and downward displacements, following
soil saturation during the hydrological cycle.

6   Conclusions

In this paper, the authors have presented a proportion of the existing literature review within the
subject area of assessment and health monitoring of masonry arch bridges. The history of masonry
arch bridges, their architecture and the factors affecting their structural integrity have been reported.

The main methods for the assessment and monitoring of masonry bridges in terms of the location of
defects and deformities using conventional methods and techniques were highlighted. Following
this, a section was dedicated to presenting a summary of the main non-destructive testing (NDT)
methods and the available research based outputs and their application.

The paper has also highlighted the viability of the utilisation of NDT methods in this area of endeavour. The importance of adopting new and more advanced monitoring strategies and techniques for effective conservation of structural features within the context of safeguarding the cultural heritage has been emphasised upon. To that effect, a novel "integrated" holistic health monitoring approach including the Ground Penetrating Radar (GPR) and the Interferometric Synthetic Aperture Radar (InSAR) techniques has been proposed and applied.

Results of these investigations produced vital information concerning the structural integrity of the "Old Bridge" at Aylesford, Kent, UK.

In more detail, GPR was essential in providing structural detailing of the bridge deck geometry. This was effected by using a high frequency antenna system (2000 MHz central frequency) allowing to establish and map the thickness of the tarmac layer as well as the under layers (bridge deck surface cover) and providing information about the total depth of the bridge deck above the historic stonework. These are crucial details for the identification of the non-homogeneous areas within the bridge superstructure. In addition, use of a low-frequency antenna system (200 and 600 MHz central frequencies) allowed to identify and locate the exact positioning of the structural ties.

Regarding the use of the InSAR technique, observations involved a period of 21 months. Results highlighted a clear matching between seasonal trends of displacements of permanent scatterers (PSs) located in the vicinity of the bridge and the flood trends recorded by the two nearest downstream stations to the bridge location. Coherence in the displacement trend for all the identified scatterers has proved the influence of the entire bridge structure to a cyclic sequence of upward and downward displacements, following soil saturation during the hydrological cycle.

This "integrated" holistic approach for the structural health monitoring of an ancient masonry bridge (the Old Bridge) proved particularly useful which in turn could be utilised and applied to similar structures.

It is believed that, this research has contributed and added value to the existing knowledge within the context of understanding the behaviour of structures such as bridges of historical and cultural values under dynamic and static conditions.

References

[1] Galliazzo V. I ponti romani. Catalogo generale. Treviso: Edizioni Canova, 1994.

[2] Watson C, Watson T, Coleman R. Structural monitoring of cable-stayed bridge: analysis of GPS versus modeled deflections. J Survey Eng 2007;133:23–28. https://doi.org/10.1155/2013/947867

[3] Moschas F, Stiros S. Measurement of the dynamic displacements and of the modal frequencies of a short-span pedestrian bridge using GPS and an accelerometer. Eng Struct 2011;33:10–17. https://doi.org/10.1061/(ASCE)0733-9453(2007)133:1(23)

[4] Zhou G-D, Yi T-H. Recent developments on wireless sensor networks technology for bridge health monitoring. Math Prob Eng 2013;947867. https://doi.org/10.1155/2013/947867

[5] Alani AM, Aboutalebi M, Kilic G. Integrated health assessment strategy using NDT for reinforced concrete bridges, NDTE Int 2014;61:80-94. https://doi.org/10.1016/j.ndteint.2013.10.001

[6] Pieraccini M, Parrini F, Fratini M, Atzeni C, Spinelli P, Micheloni M. Static and dynamic testing of bridges through microwave interferometry. NDTE Int 2007;40:208–214. https://doi.org/10.1016/j.ndteint.2006.10.007Get rights and content

[7] Gentile, C. Deflection measurement on vibrating stay cables by non-contact microwave interferometer. NDTE Int 2010;43:231–240. https://doi.org/10.1016/j.ndteint.2009.11.007

[8] Melville BW, Coleman SE. Bridge Scour. Water Resources Publications, LLC, Colorado, USA, 2000.

[9] Briaud JL, Ting F, Chen HC, Cao Y, Han SW, Kwak K. Erosion function apparatus for scour rate predictions. J Geotech Geoenviron 2001;127(2):105-113. https://doi.org/10.1061/(ASCE)1090-0241(2001)127:2(105)

[10] Hamill L. Bridge hydraulics. London: E and FN Spon; 1999.

[11] Prendergast LJ, Gavin K. A review of bridge scour monitoring techniques, J Rock Mech Geotech 2014;6(2):138-149. https://doi.org/10.1016/j.jrmge.2014.01.007

[12] Shirole AM, Holt RC. Planning for a comprehensive bridge safety assurance program. Transp Res Rec, Washington DC (1991), pp. 137-142.

[13] Briaud JL, Chen H, Li Y, Nurtjahyo P, Wang J. SRICOS-EFA method for contraction scour in fine-grained soils. J Geotech Geoenviron 2005;131(10):1283-1294. https://doi.org/10.1061/(ASCE)1090-0241(2005)131:10(1283)

[14] Ferretti A, Prati C, Rocca F. Permanent scatterers in SAR interferometry. IEEE Trans Geosci Remote Sens 2001;39:8–20. doi: 10.1109/IGARSS.1999.772008

[15] Berardino P, Fornaro G, Lanari R, Sansosti E. A new algorithm for surface deformation monitoring based on small baseline differential SAR interferograms. IEEE Trans Geosci Remote Sens 2002;40:2375–2383. doi: 10.1109/TGRS.2002.803792

[16] Massonnet D, Feigl K, Rossi M, Adragna F. Radar interferometric mapping of deformation in the year after the Landers earthquake. Nature 1994;369:227–230. https://doi.org/10.1038/369227a0

[17] Jung J, Kim D-J, Palanisamy Vadivel SK, Yun S-H. Long-term deflection monitoring for bridges using X and C-band time-series SAR interferometry. Remote Sens 2019;11(11):1258. https://doi.org/10.3390/rs11111258

717 [18] Bianchini Ciampoli L, Gagliardi V, Clementini C, Latini D, Del Frate F, Benedetto A. transport
718 infrastructure monitoring by InSAR and GPR data fusion. Surv Geophys 2019.
719 https://doi.org/10.1007/s10712-019-09563-7

720 [19] Tosti F, Gagliardi V, D'Amico F, Alani AM. Transport infrastructure monitoring by data fusion
721 of GPR and SAR imagery information. Transp Res Proc 2020;45:771-778.
722 https://doi.org/10.1016/j.trpro.2020.02.097

723 [20] Fornaro G, Reale D, Verde S. Monitoring thermal dilations with millimetre sensitivity via multi-
724 dimensional SAR imaging. In: Proceedings of the 2012 Tyrrhenian Workshop on Advances in Radar
725 and Remote Sensing (TyWRRS), Naples, Italy; Sept. 2012. p. 131–5.

726 [21] Goel K, Rodriguez Gonzalez F, Adam N, Duro J, Gaset M. 2014. Thermal dilation monitoring of
727 complex urban infrastructure using high resolution SAR data. In: Proceedings of the 2014 IEEE
728 Geoscience and Remote Sensing Symposium (IGARSS), Quebec City, QC, Canada; July 2014. p. 954–
729 7.

730 [22] Bianchini Ciampoli L, Gagliardi V, Calvi A, D'Amico F, Tosti F. Automatic network-level bridge
731 monitoring by integration of InSAR and GIS catalogues. In: Proceedings of SPIE - The International
732 Society for Optical Engineering, 11059. Munich, Germany; June 2019.
733 https://doi.org/10.1117/12.2527299

734 [23] Del Soldato M, Tomás R, Pont J, Herrera G, Lopez-Davalillos JCG, Mora O., 2016. A multi-sensor
735 approach for monitoring a road bridge in the Valencia harbor (SE Spain) by SAR Interferometry
736 (InSAR). Rend Online Soc Geol Ital 2016;41:235–238. https://doi.org/10.3301/ROL.2016.137

737 [24] D'Amico F, Gagliardi V, Bianchini Ciampoli L, Tosti F, 2020. Integration of InSAR and GPR
738 techniques for monitoring transition areas in railway bridges. NDTE Int (this issue).

739 [25] Pipinato A. Masonry bridges. In Pipinato A, editor. Innovative bridge design handbook:
740 construction, rehabilitation and maintenance. Butterworth-Heinemann; 2015.

741 [26] Fernandez Troyano L Bridge Engineering: A Global Perspective. Thomas Telford; 2003.

742 [27] UIC Code 778-3R. Recommendations for the inspection, assessment and maintenance of
743 masonry arch bridges. Paris, France, 2018.

744 [28] Heyman J. The stone skeleton. Cambridge: Cambridge University Press; 1997.

745 [29] Lourenço PB. Computational strategies for masonry structures. PhD Thesis, Delft University,
746 1996.

747 [30] Sarhosis V, De Santis S, De Felice G. A review of experimental investigations and assessment
748 methods for masonry arch bridges. Struct Infrastruct E 2016;12(11):1439–1464. doi:
749 10.1080/15732479.2015.1136655

750 [31] Proske D, van Gelder P. Safety of historical stone arch bridges. Germany: Springer-Verlag Berlin
751 Heidelberg; 2009.

752 [32] Hola J, Schabowicz K. State-of-the-art non-destructive methods for diagnostic testing of
753 building structures – anticipated development trends. Arch Civ Mech Eng 2010;10(3):5-18.
754 https://doi.org/10.1016/S1644-9665(12)60133-2

[33] Berndt E, Schöne I. Tragverhalten von Natursteinmauerwerk aus Elbesandstein. Sonderforschungsbereich 315, Universität Karlsruhe, 1990.

[34] Vicente R, Ferreira TM, Mendes da Silva JA, Varum H. In situ flat-jack testing of traditional masonry walls: case study of the old city center of Coimbra, Portugal. Int J Archit Herit 2015;9(5):794-810. https://doi.org/10.1080/15583058.2013.855840

[35] Bindia L, Tiraboschi C. Flat-jack test: a slightly destructive technique for the diagnosis of brick and stone masonry structures, 1999.

[36] Colla C, Das PC, McCann D, Forde MC. Sonic, electromagnetic and impulse radar investigation of stone masonry bridges. NDTE Int 1997;30(4):249-254. https://doi.org/10.1016/S0963-8695(96)00067-9

[37] McCann DM, Forde MC. Review of NDT methods in the assessment of concrete and masonry structures. NDTE Int 2001;34:71-84. https://doi.org/10.1016/S0963-8695(00)00032-3

[38] Alani AM, Tosti F, Banks K, Bianchini Ciampoli L, Benedetto A. Non-destructive assessment of a historic masonry arch bridge using ground penetrating radar and 3D laser scanner. In: Proceedings of the IMEKO International Conference on Metrology for Archaeology and Cultural Heritage (METROARCHAEO2017), Lecce, Italy; Oct 2017.

[39] AA.VV. Review on the NDTs for inspecting masonry walls. Retrieved from DISWall - Developing Innovative Systems for reinforced Masonry Walls: http://diswall.dic.unipd.it/Results/D5.2_FINAL.pdf. 2006

[40] Williamson PR. A guide to limits of resolution imposed by scattering in ray tomography. Geophysics 1991;56:202-207. https://doi.org/10.1190/1.1443032

[41] Biernat K, Idziaszek-Gonzalez A, Nita K, Sikora J, Wojtowicz S. Nondestructive Impendance Method of Brickwork Damp Identification. In Proceedings of the 42nd International Conference and NDT Exhibition NDE for Safety/Defektoskopie. Seč u Chrudimi, Czech Republic; 2012.

[42] Hola J, Matkowski Z, Schabowicz K, Sikora J, Nita K, Wojtowicz S. Identification of moisture content in brick walls by means of impedance tomography. COMPEL – Int J Comput Math Electr Electr 2012;31(6):1774-1792. https://doi.org/10.1108/03321641211267119

[43] Fauchard C, Antoine R, Bretar F, Lacogne J, Fargier Y, Maisonnave C, Pierrot-Deseilligny M. Assessment of an ancient bridge combining geophysical and advanced photogrammetric methods: Application to the Pont De Coq, France. J Appl Geophys 2013;98:100-112. https://doi.org/10.1016/j.jappgeo.2013.08.009

[44] Bungey JH, Grantham MG, Millard S. Testing of concrete in structures. Crc Press; 2006.

[45] Benedetto A, Pajewski L. Civil Engineering Applications of Ground Penetrating Radar. Springer Transactions in Civil and Environmental Engineering, 2015.

[46] Daniels DJ, Ground Penetrating Radar, 2nd ed., London, U.K.: Inst. Elect. Eng; 2004.

[47] Solla M, Laguela S, Riveiro B, Lorenzo H. Non-destructive testing for the analysis of moisture in the masonry arch bridge of Lubians (Spain). Struct Control Hlth 2013;20:1366-1376. https://doi.org/10.1002/stc.1545

[48] Orban Z, Yakovlev G, Pervushin G. Non-Destructive Testing of masonry arch bridges – an overview. Bautechnik 2008;85(10):711-717. https://doi.org/10.1002/bate.200890136

[49] Lubowiecka I, Armesto J, Arias P, Lorenzo H. Historic bridge modelling using laser scanning, ground penetrating radar and finite element methods in the context of structural dynamics, Eng Struct 2009;31(11):2667-2676. https://doi.org/10.1016/j.engstruct.2009.06.018

[50] Riveiro B, Arias P, Armesto J, Rial F, Solla M. Multidisciplinary approach to historical arch bridges documentation, ISPRS Vol. XXXVII, 2008, pp. 247-252.

[51] Perna S, Wimmer C, Moreira J, Fornaro G. X-band airborne differential interferometry: results of the OrbiSAR campaign over the Perugia area. IEEE Trans Geosci Remote Sens, 2008;46(2):489–503. doi: 10.1109/TGRS.2007.908871

[52] Perna S, Esposito C, Amaral T, Berardino P, Jackson G, Moreira J et al. The InSAeS4 airborne X-band interferometric SAR system: a first assessment on its imaging and topographic mapping capabilities. Remote Sens, 2016;8(1):40. https://doi.org/10.3390/rs8010040

[53] Perna S, Alberti G, Berardino P, Bruzzone L, Califano D, Catapano I et al. The ASI integrated sounder-SAR system operating in the UHF-VHF bands: first results of the 2018 helicopter-borne morocco desert campaign. Remote Sens, 2019;11(16):1845. https://doi.org/10.3390/rs11161845

[54] Rosen PA, Hensley S, Wheeler K, Sadowy G, Miller T, Shaffer S, et al. UAVSAR: a new NASA airborne SAR system for science and technology research. In: Proceedings of the 2006 IEEE Conference on Radar, Verona, NY, USA; April 2006.

[55] Ferretti A, Prati C, Rocca F. Nonlinear subsidence rate estimation using permanent scatterers in differential SAR interferometry. IEEE Trans Geosci Remote Sens, 2000;38(5):2202–2212. https://doi.org/10.1109/36.868878.

[56] Colesanti C, Ferretti A, Novali F, Prati C, Rocca F. SAR monitoring of progressive and seasonal ground deformation using the Permanent Scatterers Technique. IEEE Trans Geosci Remote Sens, 2003;41(7):1685-1701.

[57] Daniels DJ. Surface-penetrating radar. Electron Commun Eng, 1996;8(4):165-182. doi: 10.1049/ecej:19960402

[58] Benedetto A, Tosti F, Bianchini Ciampoli L, D'Amico F. An overview of ground-penetrating radar signal processing techniques for road inspections. Signal Process, 2017;132:201-209. https://doi.org/10.1016/j.sigpro.2016.05.016

[59] Bianchini Ciampoli L, Artagan S, Tosti F, Gagliardi V, Alani AM, Benedetto A. A comparative investigation of the effects of concrete sleepers on the GPR signal for the assessment of railway ballast. In: Proceedings of the 17th International Conference on Ground Penetrating Radar (GPR).2018. doi:10.1109/icgpr.2018.8441588

[60] Rhazi J, Dous O, Ballivy G, Laurens S, Balayssac JP. Non destructive health evaluation of concrete bridge decks by GPR and half cell potential techniques. In: Proceedings of 6th International Conference on Nondestructive Testing in Civil Engineering. Berlin, 2003.

[61] Parrillo R, Roberts R. Bridge deck condition assessment using ground penetrating radar. In: Proceedings of the ECNDT. Berlin, 2006.

[62] Benedetto A, Manacorda G, Simi A, Tosti F. Novel perspectives in bridge inspections using GPR. Nondestruct Test Eva, 2012;27(3):239–251. https://doi.org/10.1080/10589759.2012.694883

[63] Alani AM, Aboutalebi M, Kilic G. Applications of ground penetrating radar (GPR) in bridge deck monitoring and assessment. J App Geophys, 2013;97:45-54. https://doi.org/10.1016/j.jappgeo.2013.04.009

[64] Plati C, Loizos A, Gkyrtis K. Assessment of modern roadways using non-destructive geophysical surveying techniques. Surv Geophys, 2019. https://doi.org/10.1007/s10712-019-09518-y

[65] Tosti F, Ferrante C. Using ground penetrating radar methods to investigate reinforced concrete structures. Surv Geophys, 2019. https://doi.org/10.1007/s10712-019-09565-5

[66] Solla M, Lorenzo H, Riveiro B, Rial FI. Non-destructive methodologies in the assessment of the masonry arch bridge of Traba, Spain. Eng Fail Anal, 2011;18(3):828-835. https://doi.org/10.1016/j.engfailanal.2010.12.009

[67] Haeni FP, Placzek G, Trent RE. Use of ground penetrating radar to investigate refilled scour holes at bridge foundations, In: Proceedings of the Fourth International Conference on Ground Penetrating Radar, pp. 285–292. Rovaniemi, Finland, June 1992.

[68] Diamanti N, Giannopoulos A, Forde MC. Numerical modelling and experimental verification of GPR to investigate ring separation in brick masonry arch bridges. NDTE Int, 2008;41:354-363. https://doi.org/10.1016/j.ndteint.2008.01.006

[69] Loizos A, Plati C. Accuracy of ground penetrating radar horn-antenna technique for sensing pavement subsurface. IEEE Sens J 2007;7(5):842–850. doi: 10.1109/JSEN.2007.894152

[70] Saarenketo T. NDT Transportation. In H. M. Jol (Ed.), Ground penetrating radar theory and applications. Elsevier; 2009.

[71] Conde B, Ramos LF, Oliveir DV, Riveiro B, Solla M. Structural assessment of masonry arch bridges by combination of non-destructive testing techniques and three-dimensional numerical modelling: application to Vilanova bridge. Eng Struct, 2017;148:621-638. https://doi.org/10.1016/j.engstruct.2017.07.011

[72] Bergamo O, Campione G, Donadello S, Russo G. In-situ NDT testing procedure as an integral part of failure analysis of historical masonry arch bridges. Eng Fail Anal, 2015;57:31-55. https://doi.org/10.1016/j.engfailanal.2015.07.019

[73] Moro M, Saroli M, Stramondo S, Bignami C, Albano M, Falcucci E. et al. New insights into earthquake precursors from InSAR. Sci Rep, 2017;7:12035. https://doi.org/10.1038/s41598-017-12058-3

[74] Dammann DO, Eriksson LEB., Mahoney AR., Stevens CW., Van der Sanden J, Eicken H, Meyer FJ, Tweedie CE. Mapping arctic bottomfast sea ice using SAR interferometry. Remote Sens, 2018;10(5):720. https://doi.org/10.3390/rs10050720

[75] Guo Q, Xu C, Wen Y, Liu Y, Xu G. The 2017 noneruptive unrest at the Caldera of Cerro Azul Volcano (Galápagos Islands) revealed by InSAR observations and geodetic modelling. Remote Sens, 2019;11(17):1992. https://doi.org/10.3390/rs11171992

[76] Del Soldato M, Solari L, Poggi F, Raspini F, Tomás R, Fanti, R, Casagli, N. Landslide-induced damage probability estimation coupling InSAR and field survey data by fragility curves. Remote Sens, 2019;11(12):1486. https://doi.org/10.3390/rs11121486

[77] Gabriel AK, Goldstein RM, Zebker HA. Mapping small elevation changes over large areas: differential radar interferometry. J Geophys Res, 1989;94(B7):9183-9191. https://doi.org/10.1029/JB094iB07p09183

[78] Massonnet D, Feigl KL. Radar interferometry and its application to changes in the Earth's surface. Rev Geophys, 1998;36(4):441-500. https://doi.org/10.1029/97RG03139

[79] Rosen PA, Hensley S, Joughin IR, Li FK, Madsen SN, Rodriguez E, Goldstein RM. Synthetic aperture radar interferometry. Proc. IEEE, 2000;88(3): 333-382. doi: 10.1109/5.838084

[80] Bamler R, Hartl P. Synthetic aperture radar interferometry. Inverse Probl, 1998;14:R1-R54. https://doi.org/10.1088/0266-5611/14/4/001

[81] Lanari R, Casu F, Manzo M, Lundgren P. Application of the SBAS-DInSAR technique to fault creep: a case study of the Hayward fault, California. Remote Sens Environ,2007;109(1):20–28. https ://doi.org/10.1016/j. rse.2006.12.003

[82] Lanari R, Mora O, Manunta M, Mallorqui JJ, Berardino P, Sansosti E. A small-baseline approach for investigating deformations on full-resolution differential SAR interferograms. IEEE Trans Geosci Remote Sens, 2004;42(7):1377–1386. doi:10.1109/tgrs.2004.828196

[83] Casu F, Manzo M, Lanari R. A quantitative assessment of the SBAS algorithm performance for surface deformation retrieval from DInSAR data. Remote Sens Environ, 2006;102(3-4):195–210. https://doi.org/10.1016/j.rse.2006.01.023

[84] Lanari R, Lundgren P, Manzo M, Casu F. Satellite radar interferometry time series analysis of surface deformation for Los Angeles, California. Geophys Res Lett, 2004;31(23). https://doi.org/10.1029/2004GL021294

[85] Colesanti C, Ferretti A, Prati C, Rocca F. Monitoring landslides and tectonic motions with the Permanent Scatterers Technique, Eng Geol, 2003;68:3–14. https://doi.org/10.1016/S0013-7952(02)00195-3

[86] Colesanti C, Mouelic SL, Bennani M, Raucoules D, Carnec C, Ferretti A. Detection of mining related ground instabilities using the Permanent Scatterers technique—a case study in the east of France. Int J Remote Sens, 2005;26(1):201-207. https://doi.org/10.1080/0143116042000274069

[87] Milillo P, Giardina G, Perissin D, Milillo G, Coletta A, Terranova C. Pre-collapse space geodetic observations of critical infrastructure: the Morandi Bridge, Genoa, Italy. Remote Sensing, 2019;11(12):1403. https://doi.org/10.3390/rs11121403

[88] Koudogbo F, Urdiroz A, Robles JG, Chapron G, Lebon G, Fluteaux V, Priol G. Radar interferometry as an innovative solution for monitoring the construction of the Grand Paris Express metro network—first results. In: World tunnel conference, 2–25 April, 2018, Dubai.

[89] Barla G, Tamburini A, Del Conte S, Giannico C. InSAR monitoring of tunnel induced ground movements. Geomechanik und Tunnelbau, 2016;9(1):15–22. https ://doi.org/10.1002/geot.20150 0052

908 [90] Yang Z, Schmid F, Roberts C. Assessment of railway performance by monitoring land
909 subsidence.In: 6th IET conference on railway condition monitoring (RCM 2014), pp 1–6, 2014. https
910 ://doi.org/10.1049/cp.2014.1000

911 [91] Sarmap. SARscape technical description. http://www.sarmap.ch/pdf/ /SARscapeTechnical.pdf/;
912 2012 [accessed 11 February 2020].

913 [92] Sarmap. SAR-Guidebook, http://www.sarmap.ch/pdf/SAR-Guidebook.pdf; 2009 [accessed 11
914 February 2020].

915 [93] ENVI SARscape Brochure,
916 https://www.harrisgeospatial.com/Portals/0/pdfs/HG_SARscape_brochure_WEB.pdf [accessed 11
917 February 2020].

918 [94] NASA, The Shuttle Radar Topography Mission (SRTM) Collection User Guide.
919 https://lpdaac.usgs.gov/documents/179/SRTM_User_Guide_V3.pdf; 2015 [accessed 11 February
920 2020].

921 [95] Rodriguez E, Morris CS, Belz JE, Chapin EC, Martin JM, Daffer W, Hensley S. An assessment of
922 the SRTM topographic products, Technical Report JPL D-31639, Jet Propulsion Laboratory,
923 Pasadena, California, 143 pp., 2005.

924 [96] National River Flow Archive; 2019, https://nrfa.ceh.ac.uk, UK Centre for Ecology & Hydrology
925 (UKCEH), Wallingford. [accessed 10 October 2019].